AIAA SciTech Forum
12-16 January 2026, Orlando, FL
AIAA SCITECH 2026 Forum

10.2514/6.2026-0551

Multi-Objective Synthesis of Hybrid Incremental Dynamic Inversion Control Laws Using $\mathcal{H}_\infty$ Loop-Shaping

Leonardo Encarnação*
Institute of Flight Systems, German Aerospace Center (DLR), 82234 Weßling, Germany
Delft University of Technology, Kluyverweg 1, 2629 HS Delft, The Netherlands

Tijmen Pollack †, Spilios Theodoulis‡
Delft University of Technology, Kluyverweg 1, 2629 HS Delft, The Netherlands

Gertjan Looye§
Institute of Flight Systems, German Aerospace Center (DLR), 82234 Weßling, Germany

Nonlinear Dynamic Inversion (NDI) control and its Incremental variant (INDI) provide a conceptually simple and modular control framework, making it an attractive technique for designing flight control laws. By coupling these control architectures with robust control synthesis procedures, the overall approach can systematically ensure compliance with certification-level robustness requirements. In this sense, the $\mathcal{H}_\infty$ Loop-Shaping Design Procedure (LSDP) is a strong contender as a robust control synthesis approach, as it provides controllers with a priori robust stability guarantees. Therefore, in this study, structured $\mathcal{H}_\infty$ synthesis based on the $\mathcal{H}_\infty$ LSDP is used to systematize the development of (I)NDI control laws. This has been made possible by the advent of non-smooth non-convex multi-objective $\mathcal{H}_\infty$ optimization with MATLAB® `systune`. Despite the inherently nonlinear nature of (I)NDI-based control laws, local stability and robustness can be assessed using established trim-and-linearize techniques, allowing LTI methodologies to address design trade-offs in alignment with well established practices. Consequently, a linear hybrid Incremental Dynamic Inversion (IDI) control architecture is proposed, combining linear model-based DI with sensor-based IDI to leverage their complementary robustness properties. Model-following requirements are included using a weighting filter, whose parameters are optimized together with the hybrid IDI controller via a co-design approach. The potential of the proposed methodology is assessed in a design case study focused on a digital pitch-rate controller for a simulation model of NASA's X-29 experimental aircraft. Results demonstrate that the synthesis procedure allows to optimize hybrid IDI controllers with the robustness guarantees associated with the $\mathcal{H}_\infty$ Loop-Shaping setup while simultaneously allowing to meet performance requirements.

I. Introduction

Nonlinear Dynamic Inversion (NDI) and $\mathcal{H}_\infty$ Loop-Shaping are two popular control techniques that found application in the field of flight controls [1, 2]. However, they are the result of fundamentally different philosophies. While NDI can be deemed a flight physical approach to flight control, $\mathcal{H}_\infty$ Loop-Shaping is anchored in a theoretical frequency-domain control synthesis method. As a result, these methods target different aspects of control law design.

Nonlinear Dynamic Inversion (NDI) control laws appeared as an alternative to the divide-and-conquer paradigm associated with linear control, which typically involves gain scheduling based on local linear designs of LTI systems obtained from the Jacobian linearization of the nonlinear dynamics around chosen operating points. NDI incorporates an onboard model (OBM) representation of the airframe dynamics and uses it to invert the dynamics in a closed-loop fashion. It enables the decoupling of the control design's airframe-dependent and flying qualities-dependent parts [3, 4].

*Research Associate, Department Flight Control and Simulation, leonardo.silvaencarnacao@dlr.de
previously: MSc. Student, Control & Simulation Section, Faculty of Aerospace Engineering
†Postdoctoral Researcher, Aerospace Structures and Materials Department, Faculty of Aerospace Engineering, t.s.c.pollack@tudelft.nl
‡Associate Professor, Faculty of Aerospace Engineering, Department Control & Simulation, s.theodoulis@tudelft.nl, AIAA Associate Fellow
§Head of Department, Department of Control of Aeroelastic Systems, Institute of Aeroelasticity and Flight Control Expert, Department of Flight Control and Simulation, gertjan.looye@dlr.de

Therefore, it can be seen as a transparent and modular approach to flight control design, allowing re-use and easier adaptation of the control design across different flight control problems [1, 5]. However, NDI-based control laws come with several challenges of their own, namely the absence of inherent robustness guarantees [6] and the necessity for precision and accuracy of the OBM, since an unreliable OBM can lead to poor dynamic inversion and, consequently, poor flight control system performance [7]. Furthermore, as the aerospace industry certification requirements are often based on linear methods, such as gain and phase margins, NDI control laws needs to be evaluated in this context. This can be achieved by linearizing the closed-loop system with the plant and the controller across multiple flight conditions of the flight envelope and inspecting robustness margins. The fact that NDI aims to approach the control problem from a 'global' perspective, but robustness is fundamentally a local property, raises the question as to how to embed the required minimum robustness levels to the NDI controller.

Incremental Nonlinear Dynamic Inversion (INDI) is an incremental approach to the classical model-based (MB) NDI. This approach attempts to solve NDI's sensitivity to model errors by using sensor measurements of the derivative of the controlled variable, and hence it is also referred to as sensor-based (SB) INDI. As a result, the only onboard model information required is the plant control effectiveness, making the control law design less expensive and time-consuming. Its origin traces back to the work of [8], which refers to it as 'simplified' NDI. Dedicated flight test trials were performed to assess the potential of this new method in its initial stages, and the results turned out promising [9]. This method was further studied in terms of its potential for fault-tolerant control in [10–13]. Multiple studies have demonstrated the increased robustness of SB-INDI to uncertainty in the airframe aerodynamics, both in-simulation [14–17] and with flight tests [18–21]. Furthermore, analytical proofs of nominal and robust stability properties under external disturbances and regular perturbations have been established [22]. Nevertheless, research has also demonstrated that SB-INDI has relatively small stability robustness margins against singular perturbations, which are defined as dynamic perturbations that operate at fast time scales (high frequencies) and increase the total system order [7]. Therefore, SB-INDI is sensitive to time delays, actuator dynamics and structural mode interaction [7, 19, 23]. This has motivated interest in analyzing these effects in the stability and performance of SB-INDI-based flight control laws [23–25].

In [7], a renewed perspective is given on the robustness properties induced by different inversion strategies. This is done by employing μ-analysis tools to linear variants of those techniques, subsequently labeled Dynamic Inversion (DI) and Incremental Dynamic Inversion (IDI) control, in isolation from outer-loop design. The research demonstrates that the model-based and sensor-based inversion have complementary robustness properties, and, as such, a hybrid schematic - hybrid INDI - that combines both can be leveraged to augment the robustness properties of the inversion inner loop. This is achieved by introducing an additional augmentation element that can be used to enhance the robustness of the control law, and has been done in multiple studies [26–32]. The related design parameters can be optimized using formal synthesis methods, as demonstrated in [31, 32].

Within the realm of $\mathcal{H}_\infty$ Robust Control, $\mathcal{H}_\infty$ Loop-Shaping provides controllers with robust stability guarantees without requiring explicit uncertainty models [33]. The designer shapes the broken-loop response magnitude based on classical insights using weighting filters and then makes use of $\mathcal{H}_\infty$-synthesis to maximize robust stability against normalized coprime factor (NCF) uncertainty [33]. Therefore, this method reconciles classical control methods such as loop-shaping with $\mathcal{H}_\infty$ optimization. The method has been successfully demonstrated in flight test campaigns with helicopters [34] and with the VAAC Harrier aircraft [2, 35, 36].

The question on how to design the multiple elements of (I)NDI control laws in the face of robustness guarantees remains a promising research direction. The advent of non-convex, non-smooth formal synthesis techniques allowed solving $\mathcal{H}_\infty$-synthesis problems under structural constraints [37]. These advances allow control law structures to be specified a priori, ensuring greater flexibility in controller design. As a result, modern robust control synthesis methods facilitate the systematic robust design of structured controllers, such as PID and (I)NDI-based control laws, expanding the applicability of $\mathcal{H}_\infty$-synthesis and unlocking new possibilities for robust control in practical applications [38]. The fact that the $\mathcal{H}_\infty$ Loop-Shaping technique provides guaranteed robustness properties makes it an attractive synthesis approach to the design of (I)NDI control laws.

Therefore, the contribution of this work is the proposal of a multi-objective robust synthesis framework to design Incremental Dynamic Inversion based flight control laws based on $\mathcal{H}_\infty$ Loop-Shaping. This is achieved by employing a non-smooth non-convex multi-objective $\mathcal{H}_\infty$-synthesis in MATLAB® `systune`, which allows to directly impose structure on the controller and to optimize for both robustness and performance. Robust stability is specified via the $\mathcal{H}_\infty$ norm associated with the $\mathcal{H}_\infty$ Loop-Shaping technique, whereas nominal performance is specified in a model matching sense via a model-following weighting filter. In order to make the procedure better tailored towards dealing with multiple conflicting objectives, a co-design procedure is employed to simultaneously optimize the controller and the model-following filter parameters. The proposed methodology is demonstrated by designing a digital pitch-rate

controller for a simulation model of NASA's X-29 experimental aircraft in a severely unstable flight condition.

This paper is structured as follows: Section II provides a theoretical background on MB-NDI, SB-INDI, hybrid INDI and $\mathcal{H}_\infty$ Loop-Shaping. Section III presents a multi-objective robust synthesis methodology for tuning hybrid IDI structured controllers using the $\mathcal{H}_\infty$ Loop-Shaping Design Procedure. Section IV evaluates the methodology for the design of a digital pitch-rate controller for the X-29. Lastly, the main conclusions of this work are drawn in Section V.

II. Background

A. Nonlinear Dynamic Inversion Control

Nonlinear dynamic inversion control laws make use of the principles of feedback linearization to transform selected input-output channels into a chain of integrators of relative degree ρ. Consider the affine nonlinear system with n states and m inputs described by:

$$\Sigma: \quad \begin{cases} \dot{\boldsymbol{x}} = \boldsymbol{f}(\boldsymbol{x}) + G(\boldsymbol{x})\boldsymbol{u}, \\ \boldsymbol{y} = \boldsymbol{h}(\boldsymbol{x}), \end{cases} \tag{1}$$

where the state vector $\boldsymbol{x} \in \mathbb{R}^n$, the input vector $\boldsymbol{u} \in \mathbb{R}^m$, the observation vector $\boldsymbol{y} \in \mathbb{R}^m$, and smooth mappings $\boldsymbol{f}$, G, and $\boldsymbol{h}$. Writing the system relative degree as $\boldsymbol{\rho} = [\rho_1, \ldots, \rho_m]^T$, the output dynamics can be described as [22]:

$$\boldsymbol{y}^{(\boldsymbol{\rho})} = \begin{bmatrix} L_f^{\rho_1} h_1(\boldsymbol{x}) \\ \vdots \\ L_f^{\rho_m} h_m(\boldsymbol{x}) \end{bmatrix} + \begin{bmatrix} L_{g_1} L_f^{\rho_1 - 1} h_1(\boldsymbol{x}) & \cdots & L_{g_m} L_f^{\rho_1 - 1} h_1(\boldsymbol{x}) \\ \vdots & \ddots & \vdots \\ L_{g_1} L_f^{\rho_m - 1} h_m(\boldsymbol{x}) & \cdots & L_{g_m} L_f^{\rho_m - 1} h_m(\boldsymbol{x}) \end{bmatrix} \boldsymbol{u} \triangleq \boldsymbol{\alpha}(\boldsymbol{x}) + B(\boldsymbol{x})\boldsymbol{u} \tag{2}$$

where $L_f^k h_i(\boldsymbol{x})$ and $L_{g_i} L_f^{k-1} h_i(\boldsymbol{x})$ represent repeated Lie derivatives of the function h_i along the vector fields $\boldsymbol{f}$ and $\boldsymbol{g_i}$, with $\boldsymbol{g_i}$ being a column vector of the matrix G [39]. For traditional feedback linearization, this expression can be used directly to construct a control law that linearizes the input-output dynamics to a set of $\sum_{i=1}^{m} \rho_i$ parallel integrators. Assuming that the control effectiveness matrix $B(\boldsymbol{x})$ is invertible, the following control law is obtained:

$$\boldsymbol{u} = \hat{B}^{-1}(\boldsymbol{x}) \left[\boldsymbol{y}^{(\boldsymbol{\rho})} - \hat{\boldsymbol{\alpha}}(\boldsymbol{x}) \right]. \tag{3}$$

where the onboard model estimates of $\alpha(\boldsymbol{x})$ and $B(\boldsymbol{x})$ are represented as $\hat{\boldsymbol{\alpha}}(\boldsymbol{x})$ and $\hat{B}(\boldsymbol{x})$, respectively. Here, $\boldsymbol{\nu} \in \mathbb{R}^m$ is the pseudo-control vector generated by an auxiliary virtual control law designed to meet control objectives. The control law is illustrated in Fig. 1.

To obtain an analogous control law in incremental form, a Taylor expansion of the output dynamics around the system state at time $t - \Delta t$ can be performed [22], where Δt represents the sampling interval. Denoting this condition by the subscript 0 for ease of notation yields the expression:

$$\boldsymbol{y}^{(\boldsymbol{\rho})} = \boldsymbol{y}_0^{(\boldsymbol{\rho})} + \left. \frac{\partial [\boldsymbol{\alpha}(\boldsymbol{x}) + B(\boldsymbol{x})\boldsymbol{u}]}{\partial \boldsymbol{x}} \right|_0 \underbrace{(\boldsymbol{x} - \boldsymbol{x}_0)}_{\Delta \boldsymbol{x}} + B(\boldsymbol{x}_0) \underbrace{(\boldsymbol{u} - \boldsymbol{u}_0)}_{\Delta \boldsymbol{u}} + \boldsymbol{R}_1, \tag{4}$$

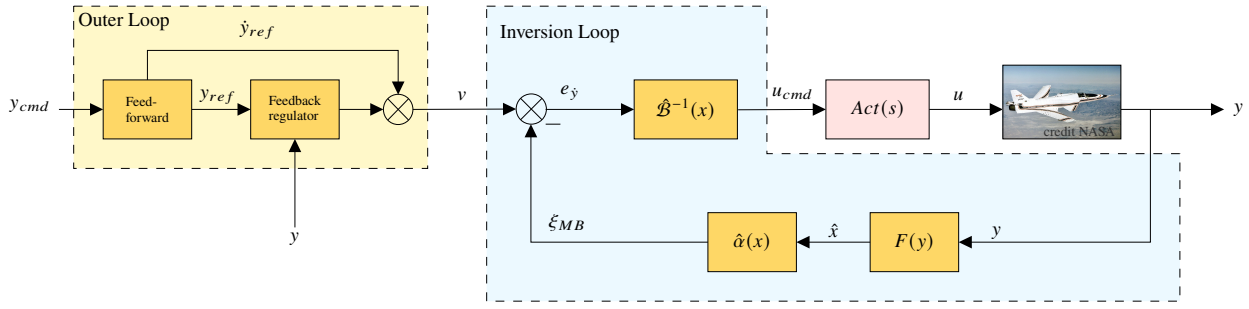

Fig. 1 Model-Based NDI schematic.

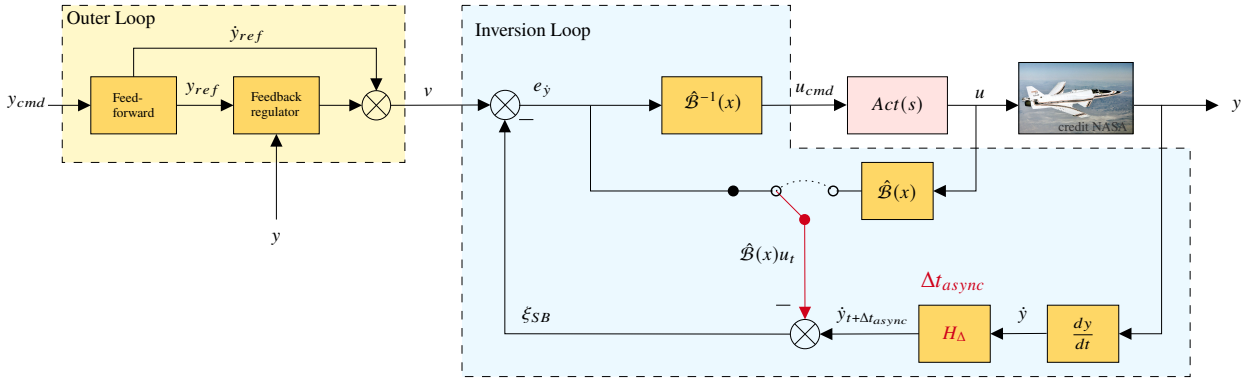

Fig. 2 Sensor-Based INDI schematic. Control Command input feedback and input sensor measurements feedback are displayed as sources of input feedback.

where $\boldsymbol{R}_1$ represents the expansion remainder. Consequently, the time-scale separation assumption can be leveraged to design the incremental control input $\Delta\boldsymbol{u}$, which assumes that all state-dependent and residual terms can be neglected [19]. This is often argued as justified in the case of high sampling rates and high-bandwidth actuators. The control law is completed by adding the control vector $\boldsymbol{u}_0$ to the resulting incremental term:

$$\boldsymbol{u} = \boldsymbol{u}_0 + \hat{B}^{-1}(\boldsymbol{x}_0)\left[\boldsymbol{\nu} - \boldsymbol{y}_0^{(\rho)}\right]. \tag{5}$$

Note that compared to its nonincremental counterpart from Equation 3, the resulting control law does not require any model information on $\boldsymbol{\alpha}(\boldsymbol{x})$ but uses only sensor feedback of the previous control vector and the derivative of the control variable instead. Throughout the remaining of the article, a system with relative degree $\rho = 1$ will be considered, such that $\boldsymbol{y}^{(\rho)} = \dot{\boldsymbol{y}}$.

As direct measurements of the derivative of the control variable (for instance, using angular accelerometers) are often either not available or quite noisy, it is typically preferred to use a filtered differentiation of $\boldsymbol{y}$, $\dot{\boldsymbol{y}} = sH_d\boldsymbol{y}$, where H_d is a low-pass filter. Furthermore, as sensors for the input signal are not always available, feedback of commanded input signals can be used instead. One can either assume ideal actuator, in which case the input signal used for feedback is equal to the commanded input $\boldsymbol{u} = \boldsymbol{u}_{cmd}$, or include an internal model of the actuators, resulting in $\boldsymbol{u} = G_{act}\boldsymbol{u}_{cmd}$. Since the control law requires feedback on $\hat{B}\boldsymbol{u}$, the following equations for commanded input and commanded input with actuator model feedback, respectively, can be leveraged:

$$\boldsymbol{u} = \boldsymbol{u}_{cmd} = \hat{B}^{-1}\boldsymbol{e}_{\dot{\boldsymbol{y}}} \Rightarrow \hat{B}\boldsymbol{u} = \boldsymbol{e}_{\dot{\boldsymbol{y}}} \tag{6}$$

$$\boldsymbol{u} = G_{act}(s)\boldsymbol{u}_{cmd} = G_{act}(s)\hat{B}^{-1}\boldsymbol{e}_{\dot{\boldsymbol{y}}} \Rightarrow \hat{B}\boldsymbol{u} = G_{act}(s)\boldsymbol{e}_{\dot{\boldsymbol{y}}} \tag{7}$$

The fact that both these sources of input feedback are locations inside the control law itself makes it conceptually simpler to implement and does not require additional sensor measurements. Nevertheless, since including an actuator model comes at the cost of increased complexity of the control law and the work of [32] suggests that little limitations in terms of robustness of the control law result from using directly commanded inputs, that is the option chosen for the rest of the article.

A key aspect for the successful implementation of SB-INDI control is addressing the 'synchronization' issue, which refers to the relative timing or phase between the sensor-based estimate of the output derivative $\dot{\boldsymbol{y}}$ and the input feedback signal [19]. The block H_Δ in Fig. 2 reflects the nominal dynamics that are not synchronized, which stems from delays introduced by anti-aliasing filters, sensors, the low-pass filter for differentiation H_d, and others [31]. In order to address this issue, the input feedback signal is synchronized by applying a filter H_c on this feedback signal. In practice, synchronization of the low-pass filter H_d is usually enough [18, 19, 31].

$$\boldsymbol{\xi}^{SB}_{filtered}(s) = H_c(s)[s\boldsymbol{y}(s) - \hat{B}\boldsymbol{u}(s)] \tag{8}$$

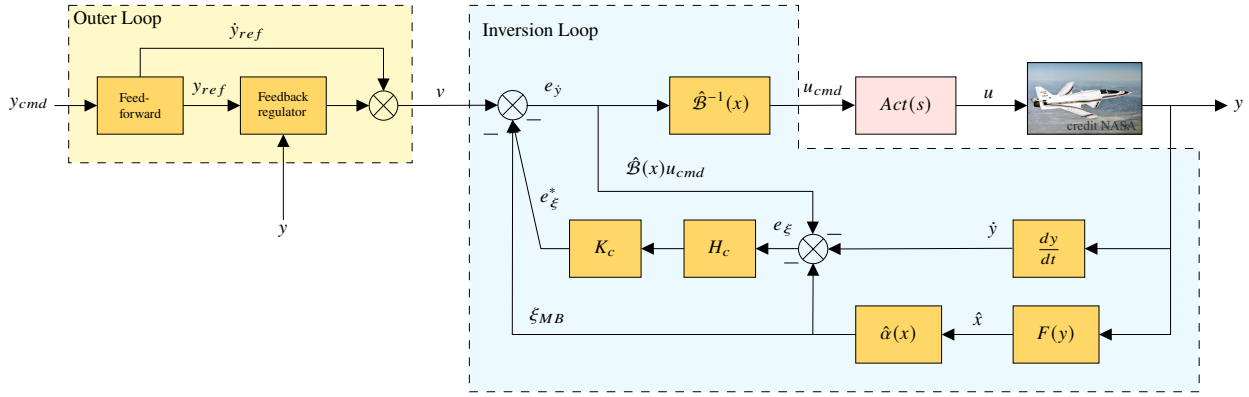

Fig. 3 Hybrid-Based INDI schematic with Control Command input feedback.

B. Elemental Robustness Properties of (I)NDI

Defining $\boldsymbol{\xi}^{MB} = \hat{\boldsymbol{\alpha}}(\boldsymbol{x})$ and $\boldsymbol{\xi}^{SB} = \dot{\boldsymbol{y}} - \hat{\boldsymbol{B}}\boldsymbol{u}_0$ as the signals in the inversion path for model-based (MB) nonlinear dynamic inversion and sensor-based (SB) incremental nonlinear dynamic inversion, respectively, the following relationship holds in the absence of On-Board model (OBM) uncertainty and disturbances [32]:

$$\underbrace{\hat{\boldsymbol{\alpha}}(\boldsymbol{x})}_{\boldsymbol{\xi}^{MB}} = \underbrace{\dot{\boldsymbol{y}} - \hat{\boldsymbol{B}}(\boldsymbol{x})\boldsymbol{u}}_{\boldsymbol{\xi}^{SB}} \tag{9}$$

However, the fact that the above equality only holds in the absence of uncertainty and disturbances is a direct indication that the different inversion schemes possess different robustness properties. The work of [7] highlights that these different robustness properties can be readily understood by analyzing the open-loop response of an MB and an SB linear dynamic inversion schematic in isolation from outer loop design. The authors demonstrate that SB inversion schemes results in a high-gain control system at the level of the bare airframe, producing an elevated open-loop frequency response compared to MB ones. The higher gain at low-frequencies translates to increased robustness to aerodynamic model uncertainties, but this increased robust performance in the low-to-medium frequencies comes at the cost of robust stability against high-frequency uncertainties. Even though synchronization filter design can successfully improve the robust stability properties of SB-INDI control, the authors of [7] demonstrate that reinstating model information in the form of a complementary augmentation element can further improve robust performance of the control law. This concept was originally proposed in [26] and formulated in [27] and [28] as a hybrid INDI approach. However, the specific blend of model-based $\boldsymbol{\xi}^{MB}$ and sensor-based $\boldsymbol{\xi}^{SB}$ inversion used in the present work originates from [31, 32] and can be defined as:

$$\begin{aligned}\boldsymbol{\xi}^{HB}(s) &= (1 - K_c H_c(s))\boldsymbol{\xi}^{MB}(s) + K_c H_c(s)\boldsymbol{\xi}^{SB}(s) \\ &= \boldsymbol{\xi}^{MB}(s) + K_c H_c(s)(\boldsymbol{\xi}^{SB}(s) - \boldsymbol{\xi}^{MB}(s)) \\ &= \boldsymbol{\xi}^{MB}(s) + K_c H_c(s)\boldsymbol{e}_{\boldsymbol{\xi}}(s)\end{aligned} \tag{10}$$

where K_c is a scaling gain $\in [0,1]$ and H_c is compensation filter set as a low-pass filter. Given the relationships in Equation 10, hybrid INDI can be interpreted as a standard model-based NDI with additional error compensation, as shown in Fig. 3. Correspondingly, hybrid INDI collapses to purely model-based design when $K_c = 0$, and $\xi^{HB}(s) \rightarrow \xi^{SB}(s)$ if $K_c = 1$ and the bandwidth of $H_c(s)$ is made sufficiently large. Since the hybrid design allows navigating between model-based and sensor-based inversion schematics, it brings an extra degree of freedom to modify the broken-loop gain response, and thus help address robustness.

C. $\mathcal{H}_\infty$ Loop-Shaping Control

The $\mathcal{H}_\infty$ LSDP, originally proposed by [33] leverages the concepts of classical Loop-Shaping and the $\mathcal{H}_\infty$ machinery to design controllers which robustly stabilize a plant with respect to Normalized Coprime Factor (NCF) uncertainty. It is a two-step procedure, where in the first step the plant is shaped with weighting filters W_1 and W_2, and in the second step, a robust controller K_∞ is computed which robustly stabilizes the shaped plant $G_s = W_2 G W_1$ with respect to NCF

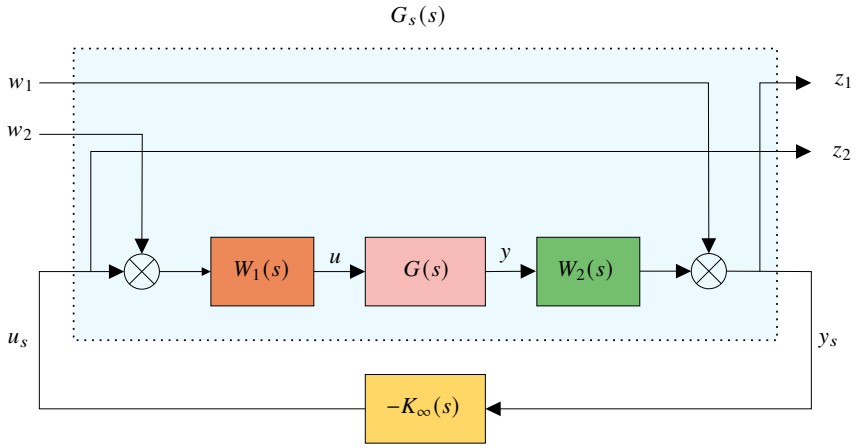

Fig. 4 NCF robust stabilization problem written as mixed sensitivity 4-block problem.

uncertainty. The first step is essential since robust stabilization alone is of limited practical value because it does not allow the designer to specify any performance requirements [40].

The robust controller K_∞ is a stabilizing controller which minimizes the following $\mathcal{H}_\infty$-norm:

$$\min_{\text{stab } K_\infty} \left\| \begin{bmatrix} w_1 \\ w_2 \end{bmatrix} \rightarrow \begin{bmatrix} z_1 \\ z_2 \end{bmatrix} \right\|_\infty = \min_{\text{stab } K_\infty} \left\| \begin{bmatrix} I_p \\ -K_\infty \end{bmatrix} \left(I_p + G_s K_\infty\right)^{-1} \begin{bmatrix} I_p & G_s \end{bmatrix} \right\|_\infty \leq \gamma \triangleq \epsilon^{-1} \tag{11}$$

The lowest achievable value $\gamma_{\min}$ is given by [41]:

$$\gamma_{\min} = \epsilon_{\max}^{-1} = \left\{ 1 - \left\| \begin{bmatrix} N & M \end{bmatrix} \right\|_H^2 \right\}^{-\frac{1}{2}} = \left(1 + \rho(XZ)\right)^{\frac{1}{2}}, \tag{12}$$

where $\| \cdot \|_H$ denotes the Hankel norm, ρ denotes the spectral radius, and X and Z are the solutions to the associated Algebraic Riccati Equations (ARE's). The suboptimal full-order K_∞ can be computed from γ, where $\gamma > \gamma_{\min}$, and the 2 ARE's. It has been demonstrated in [42] that it is possible to rewrite the NCF robust stabilization problem as a 4-block problem, where the obtained closed-loop 2×2 system is basically the transfer function from the output and input disturbance at the shaped plant $[w_1\ w_2]^T$ to $[y_s\ u_s]^T$, as shown in Fig. 4.

D. Previous Work on Combining $\mathcal{H}_\infty$ Control and NDI/INDI Control

Regarding robust NDI/INDI developments, multiple studies have concerned with establishing guidelines to design robustifying outer-loop controllers for MB-NDI control [43, 44], while other studies have focused more on analyzing the stability properties of MB-NDI controllers [6, 45]. The work of [6] on a normalized coprime factor stability test for frozen point analysis, a concept which directly ties to $\mathcal{H}_\infty$ Loop-Shaping control, is particularly relevant for the scope of the present research. This work proposes an analysis test which involves transforming the controller and the plant into an equivalent NCF controller and its corresponding weighted plant, as illustrated in Fig. 5. The goal is to determine diagonal weights W_1, W_2 such that $W_1^{-1} K W_2^{-1}$ becomes the optimal controller for the weighted plant $W_2 G W_1$. This is achieved by solving [6]:

$$\min_{W_1, W_2} \|T_{d \rightarrow e}\|_\infty = \min_{W_1, W_2} \left\| \begin{bmatrix} W_2 & \\ & W_1^{-1} \end{bmatrix} \begin{bmatrix} I \\ K \end{bmatrix} (I - GK)^{-1} \begin{bmatrix} I & G \end{bmatrix} \begin{bmatrix} W_2^{-1} & \\ & W_1 \end{bmatrix} \right\|_\infty \triangleq \frac{1}{\epsilon_\mu}, \tag{13}$$

where d consists of $[d_o\ d_i]^T$, e consists of $[y_s\ u_s]^T$, W_1, W_2 are restricted to being diagonal, stable, and minimum phase, and K is a LTI representation of a NDI/INDI controller at a certain flight condition.

A key aspect for structured $\mathcal{H}_\infty$ Loop-Shaping design is the fact that the control problem can also be interpreted as the more standard $\mathcal{H}_\infty$ problem of minimizing the $\mathcal{H}_\infty$ norm of the frequency-weighted gain from disturbances on the plant input and output to the controller input and output as originally described in [42] and illustrated in Fig. 6. To the authors knowledge, this was first used for structured $\mathcal{H}_\infty$ Loop-Shaping control synthesis, using MATLAB® hinfstruct,

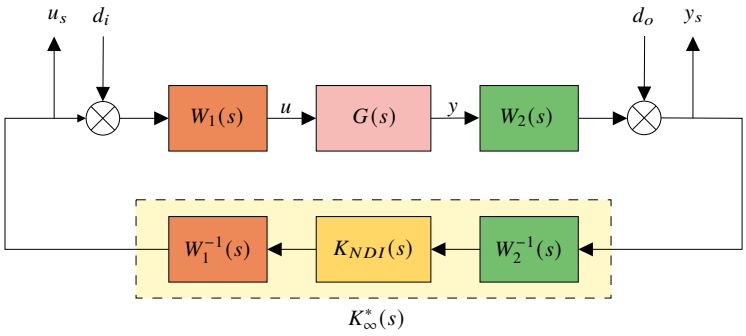

Fig. 5 Equivalent closed-loop representation with addition of "dummy" filters and their respective inverses.

in [46]. In reality, minimization of the $\mathcal{H}_\infty$-norm from $[d_o\, d_i]^T \rightarrow [y_s\, u_s]^T$ in Fig. 5 is equivalent to the one from $[w_1\, w_2]^T \rightarrow [z_1\, z_2]^T$ in Fig. 6. Thus, the setup in Fig. 5 can also be used for structured $\mathcal{H}_\infty$ Loop-Shaping synthesis.

In terms of robust control synthesis approaches to hybrid INDI control architectures, the work by [31, 32] employs a μ-synthesis approach to systematically tune a hybrid INDI controller in light of non-smooth, multi-objective $\mathcal{H}_\infty$-synthesis. Along similar lines, [47] proposes a framework for tuning a linear variant of hybrid INDI control, a hybrid IDI controller, using the $\mathcal{H}_\infty$ Loop-Shaping Design Procedure (LSDP) instead. This framework is at the core of this research and is further extended in the following sections. The recent developments by [48] establish quasi-LPV (q-LPV) model formulations of the hybrid INDI control law which enable systematic tuning over wide operating regimes and also allow LPV analysis of nonlinear stability and performance.

III. Structured Multi-Objective Robust Synthesis Using $\mathcal{H}_\infty$ Loop-Shaping

A. Equivalent $\mathcal{H}_\infty$ Loop-Shaping Setup

In [42], the authors demonstrate that the classical $\mathcal{H}_\infty$ LSDP can equivalently be interpreted as the more standard $\mathcal{H}_\infty$ problem formulation of minimizing the $\mathcal{H}_\infty$ norm of the frequency-weighted gain from disturbances on the plant input and output to the controller input and output (see Fig. 6). In order to demonstrate this equivalence, recall that the

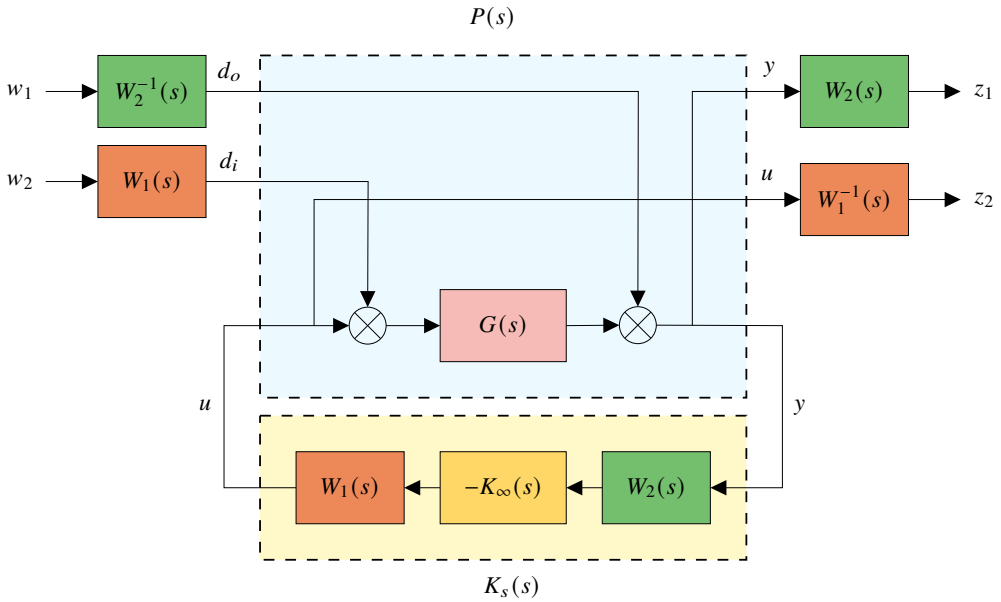

Fig. 6 Alternative structure for the $\mathcal{H}_\infty$ LSDP robust stabilization.

NCF robust stabilization problem can be written as a mixed sensitivity 4-block problem, as presented in Fig. 4 and Equation 11. The following derivation steps are retrieved from [42].

Using the fact that $G_s = W_2 G W_1$ and defining as the total controller $K_s = W_1 K_\infty W_2$, and assuming that the weighting filters are square and invertible, it is possible to rewrite Equation 11 as:

$$\left\| \begin{bmatrix} I_p \\ -K_\infty \end{bmatrix} \left(I_p + G_s K_\infty\right)^{-1} \begin{bmatrix} I_p & G_s \end{bmatrix} \right\|_\infty = \left\| \begin{bmatrix} W_2 \\ -W_1^{-1} K_s \end{bmatrix} W_2^{-1} \left(I_p + G_s K_\infty\right)^{-1} W_2 \begin{bmatrix} W_2^{-1} & G W_1 \end{bmatrix} \right\|_\infty \tag{14}$$

Using the fact that the inner part $W_2^{-1} \left(I_p + G_s K_\infty\right)^{-1} W_2$ can be written as:

$$\left[W_2^{-1} \left(I_p + W_2 G W_1 K_\infty\right) W_2\right]^{-1} = \left(I_p + G K_s\right)^{-1}, \tag{15}$$

and the following equivalence holds:

$$\left\| \begin{bmatrix} I_p \\ -K_\infty \end{bmatrix} \left(I_p + G_s K_\infty\right)^{-1} \begin{bmatrix} I_p & G_s \end{bmatrix} \right\|_\infty \leq \epsilon^{-1} \Leftrightarrow \left\| \begin{bmatrix} W_2 \\ -W_1^{-1} K_s \end{bmatrix} \left(I_p + G K_s\right)^{-1} \begin{bmatrix} W_2^{-1} & G W_1 \end{bmatrix} \right\|_\infty \leq \epsilon^{-1} \tag{16}$$

If the multiplications in Equation 16 are expanded and defining $L_s = (I_p + G K_s)^{-1}$, the following particular weighted mixed sensitivity problem is achieved:

$$\left\| \begin{bmatrix} W_2 L_s W_2^{-1} & W_2 L_s G W_1 \\ -W_1^{-1} K_s L_s W_2^{-1} & -W_1^{-1} K_s L_s G W_1 \end{bmatrix} \right\|_\infty \leq \epsilon^{-1} \tag{17}$$

The previous result can be represented as a 4-block mixed sensitivity problem with weights on the disturbances and plant input and output, as shown in Fig. 6.

$$\begin{bmatrix} z_1 \\ z_2 \end{bmatrix} = \begin{bmatrix} W_2 L_s W_2^{-1} & W_2 L_s G W_1 \\ -W_1^{-1} K_s L_s W_2^{-1} & -W_1^{-1} K_s L_s G W_1 \end{bmatrix} \begin{bmatrix} w_1 \\ w_2 \end{bmatrix} \tag{18}$$

One of the challenges of combining $\mathcal{H}_\infty$ LSDP with Dynamic Inversion control architectures is that the inversion path (inner-loop) directly closes the feedback loop with a prescribed structure. This conflicts with the 2-step nature of $\mathcal{H}_\infty$ LSDP, which first shapes the open-loop with weighting filters and only then closes the loop with the robustifying controller K_∞. However, since this 4-block representation allows to consider the disturbances and the outputs at the actual plant I/O, as opposed to the input and output of the shaped plant $G_s = W_2 G W_1$, part of the issues are overcome. The remaining issue is the fact that the weighting filters still incorporate the final feedback controller $K_s = W_1 K_\infty W_2$, which is undesirable when highly structured control architectures are considered, such as IDI controllers. Nevertheless, under Hypothesis 1, the structure can directly be imposed on the total feedback controller, namely the hybrid IDI controller, and non-smooth non-convex optimization techniques used to solve the $\mathcal{H}_\infty$ synthesis problem using MATLAB® `systune` [37]. For a representation of the optimization setup, refer to Fig. 7. Since the approach is based on LTI models of the plant's dynamics, a linear variant of a hybrid INDI controller is adopted, referred to as hybrid IDI. The controller consists of several components: the outer-loop compensator $K_v(s)$; the term $(CB)^{-1}$, which serves as the linear counterpart of $\mathcal{B}^{-1}(x)$; and CA, which represents the linear counterpart of $\alpha(x)$, both derived from the state-space model $(A, B, C, 0)$. In addition, $F(s)$ is a linear state estimator, while K_c and H_c correspond to the hybrid inversion elements introduced previously.

Hypothesis 1 *There exists a full-order controller K_∞ which minimizes the $\mathcal{H}_\infty$ norm from w to z in Fig. 7, resulting in the total controller $K_s = W_1 K_\infty W_2$. If structure is imposed on the total controller K_s, referred to as K_{struct}, then minimization of the same $\mathcal{H}_\infty$ norm from w to z in Fig. 7 results in the tunable elements of K_{struct} being reconfigured such that $K_{struct} \rightarrow K_s$ and $\gamma_{K_{strcut}} \rightarrow \gamma_{K_s}$. The underlying assumption is that the tunable elements of K_{struct} can be configured such that $K_{struct} \rightarrow K_s$.*

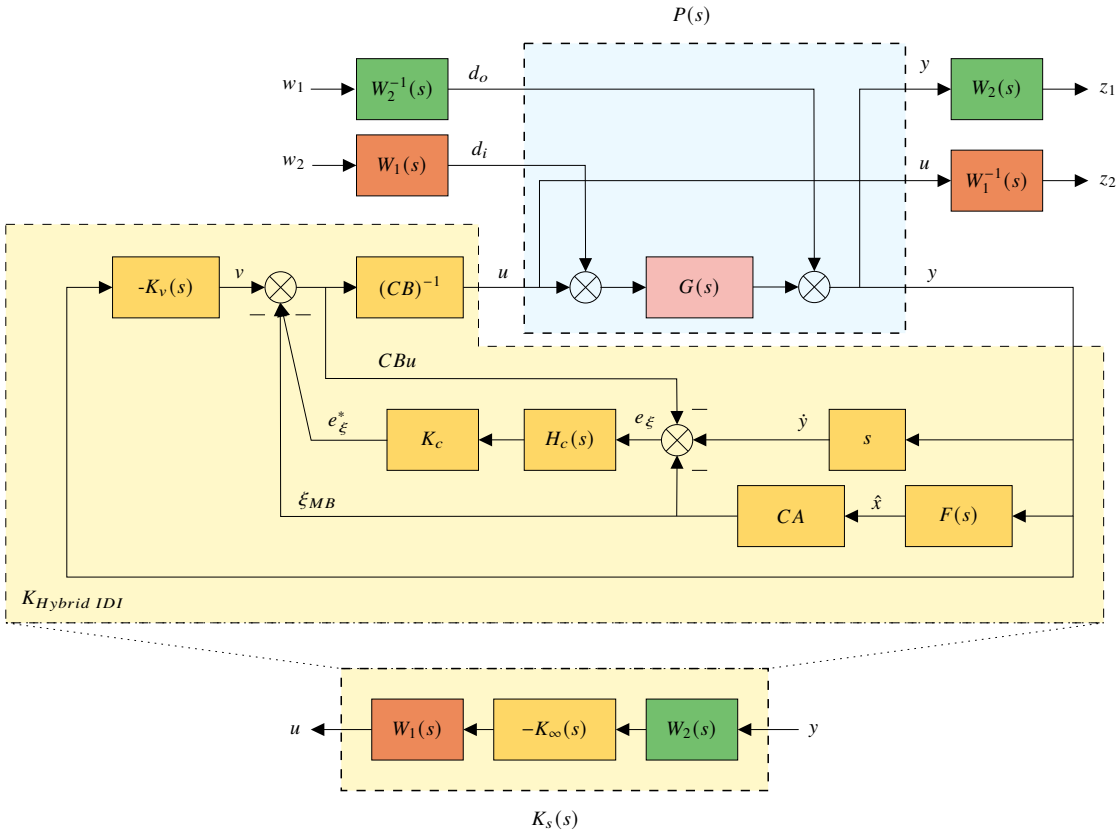

Fig. 7 Alternative structure to tune hybrid IDI controller using the $\mathcal{H}_\infty$ LSDP.

B. Incorporation of model-following specifications in two-degree-of-freedom design

Specifications for flying qualities in manual flight control systems are typically defined using the modal parameters of Low-Order Equivalent System (LOES) models [49]. These models represent the desired response of specific controlled variables to pilot inputs. LOES models are derived by simplifying high-order transfer function models that encompass the complete dynamics of the aircraft, including aerodynamics, actuator dynamics, controller dynamics, structural modes, and sensor dynamics. The LOES parameter values are generally determined based on military or other regulatory requirements to ensure the aircraft achieves satisfactory flight performance [49].

1. 2DoF Control Architecture

With respect to the 2DoF configuration depicted in Fig. 8, the feedback part K_1 is designed for nominal and/or robust stability (NS, RS) and disturbance rejection, whereas the feedforward part K_2 is for nominal and/or robust performance (NS, NP) [50]. The 'gang-of-six' closed-loop transfer functions (S_i, S_o, T_i, T_o, S_oG, KS_o) depend only on the feedback controller K_1 and determine RS with respect to all types of unstructured uncertainty [40]. The feedforward controller K_2 is used to achieve better reference tracking, since $y = T_oK_2r$, where $T_o = GK_1(I + GK_1)^{-1}$ [40].

In order to extend the procedure to a 2DoF setup, a tunable feedforward controller K_{ff} was added to the hybrid IDI structure and model following performance requirements were introduced via minimization of the $\mathcal{H}_\infty$ norm from y_{cmd} to z_3 as shown in Fig. 9.This allows to systematically trade-off robustness with model following performance, as robustness is associated with the minimization of $\mathcal{H}_\infty$ norm from $[w_1\ w_2]^T \rightarrow [z_1\ z_2]^T$ and model following performance with the $\mathcal{H}_\infty$ norm from $y_{cmd} \rightarrow z_3$. As the model following performance is made more demanding, via the W_{mf} filter, the $\mathcal{H}_\infty$ norm from $[w_1\ w_2]^T \rightarrow [z_1\ z_2]^T$ is increased, decreasing the robustness of the overall system. Therefore, directly in the synthesis part, the designer can trade off these properties. More details on the working principles of designing W_{mf} are provided in the section below.

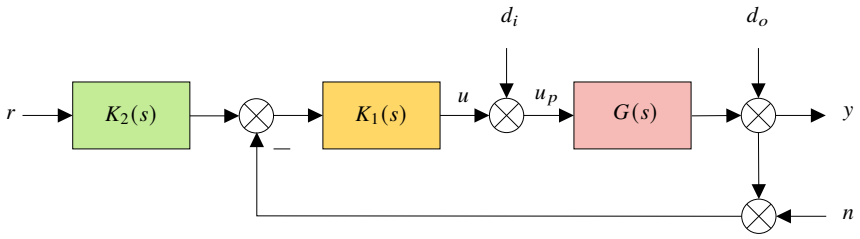

Fig. 8 2DoF control architecture.

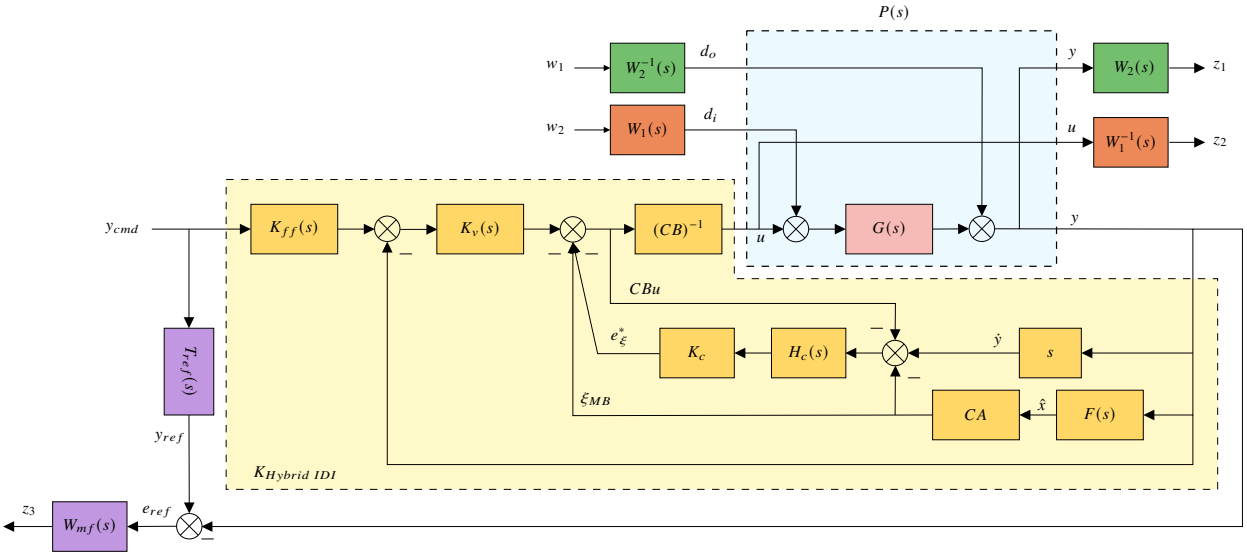

Fig. 9 2DoF Loop-Shaping Design Procedure for hybrid IDI controller structure.

2. Co-Design

As described in the section above, the inclusion of model-following requirements is achieved via a model-following filter W_{mf} on the error signal e_{ref}. In this context, it is more intuitive to interpret the relevance of W_{mf}^{-1} as it is the filter that sets the bounds for the transfer function from y_{cmd} to e_{ref}, given that:

$$\left\| \frac{z_3(s)}{y_{cmd}(s)} \right\|_\infty \leq 1 \Leftrightarrow \left\| W_{mf}(s) \left(T_{ref}(s) - \frac{y(s)}{y_{cmd}(s)} \right) \right\|_\infty \leq 1 \Leftrightarrow \left\| T_{ref}(s) - \frac{y(s)}{y_{cmd}(s)} \right\|_\infty \leq \left\| W_{mf}^{-1}(s) \right\|_\infty \tag{19}$$

The inverse of the model following filter, W_{mf}^{-1}, is a high-pass filter since the tracking commands are relevant in the low-frequency region. A first-order filter is used and can be parametrized as:

$$W_{mf}(s) = \frac{s + \omega_e M_e}{M_e(s + \omega_e A_e)} \quad \Rightarrow \quad W_{mf}^{-1}(s) = \frac{M_e(s + \omega_e A_e)}{s + \omega_e M_e} \tag{20}$$

The DC gain of W_{mf}^{-1} is given by A_e, the peak gain is given by M_e and the bandwidth with the value ω_e. The lower the DC gain and the higher the bandwidth of W_{mf}^{-1}, the better the model-following performance. The high-frequency gain typically corresponds to a frequency region beyond the relevant range, so its role is not as critical in the model-following performance.

Choosing the different filter parameters often requires managing conflicting trade-offs and might require some iterations to strike a desired balance between performance and robustness. Similarly to the work of [51], this motivated the idea of using a co-design procedure, where the model-following error weighting filter parameters are tunable parameters optimized in parallel together with the minimization of the $\mathcal{H}_\infty$ norm in Equation 19. Choosing the desired value for the DC gain is often trivial: -40 dB is often sufficient, thus, any value below that yields good steady-state

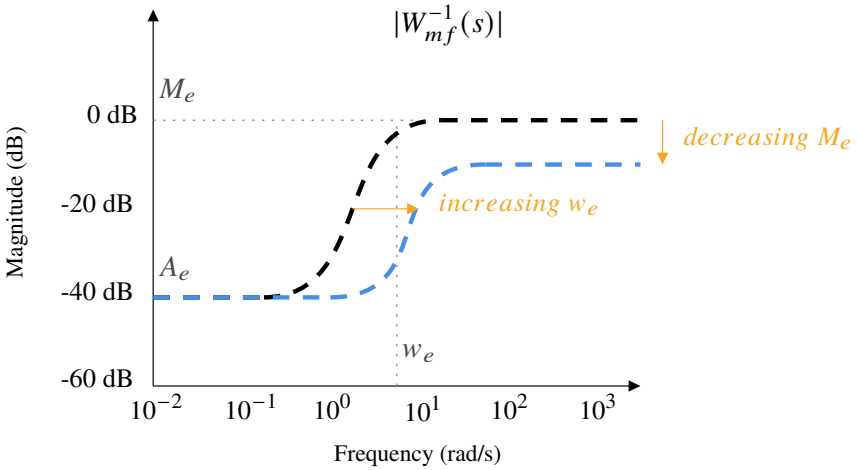

Fig. 10 Template of inverse of model-following error weighting filter W_{mf}^{-1}.

tracking. Therefore, the parameter A_e is directly set by the designer and is not part of the co-design optimization routine. The ω_e and M_e parameters are optimized such that the value of ω_e is maximized and the value of M_e is minimized, and hence, the bandwidth of W_{mf}^{-1} is maximized and its peak value minimized as displayed in Fig 10. This results in an increased demand of model-following performance.

Given the non-convex nature of the optimization in MATLAB® `systune`, it is necessary to include bounds on the values of the model-following filter tunable parameters to limit the subset of the solution space [51]. Consequently, a lower bound is defined for the value of ω_e and a certain range for the admissible values of M_e. Moreover, given the multi-objective nature of the problem, it is necessary to introduce tuning knobs as to make these performance goals more or less demanding. This is achieved by specifying a desired value for ω_e and M_e, via $\omega_{e_{goal}}$ and $M_{e_{goal}}$. It is also important to scale these objectives with respect with the NCF robustification goal (with value γ) in Equation 22, since this normally takes values around 3 and all goals should be on the same scale in order for them to be 'competitive'. This results in the following formulation of these co-design goals:

$$\min \left\| \frac{\omega_{e_{goal}}}{\omega_e} \gamma_{goal} \right\|_\infty \leq 1, \quad \min \left\| \frac{M_e}{M_{e_{goal}}} \gamma_{goal} \right\|_\infty \leq 1 \tag{21}$$

The complete multi-objective $\mathcal{H}_\infty$-synthesis problem setup can then be defined as done in Equation 22 and as visually depicted in Fig. 11.

$$\begin{aligned} \min_{\kappa} \quad & \max \left\{ \underbrace{\left\| T_{w_2 \to z_2}(K(s,\kappa)) \right\|_\infty}_{\text{Co-Design Goal for } w}, \underbrace{\left\| T_{w_3 \to z_3}(K(s,\kappa)) \right\|_\infty}_{\text{Co-Design Goal for } M}, \underbrace{\left\| T_{\left[\begin{smallmatrix} w_4 \\ w_5 \end{smallmatrix}\right] \to \left[\begin{smallmatrix} z_4 \\ z_5 \end{smallmatrix}\right]}(K(s,\kappa)) \right\|_\infty}_{\text{NCF robustification} = \gamma} \right\} \\ \text{subject to} \quad & \underbrace{\left\| T_{w_1 \to z_1}(K(s,\kappa)) \right\|_\infty \leq 1}_{\text{Model-Following Goal}} \end{aligned} \tag{22}$$

With this setup the designer can require more performance by increasing $\omega_{e_{goal}}$ and decreasing $M_{e_{goal}}$, which will increase the value of the tuned ω_e and the decrease the value of M_e, which in turn translates to a more demanding model-following error weighting filter W_{mf}^{-1}. On the other hand, if robustness is too heavily compromised, the designer can alleviate the model-following performance requirements by decreasing $\omega_{e_{goal}}$ and increasing $M_{e_{goal}}$, which will result in a lower γ value.

Under this framework, the controller $K(\kappa)$ can be selected to be any structured controller, such as the PID controllers widely celebrated in the industry or the increasingly popular Nonlinear Dynamic Inversion and Incremental Nonlinear

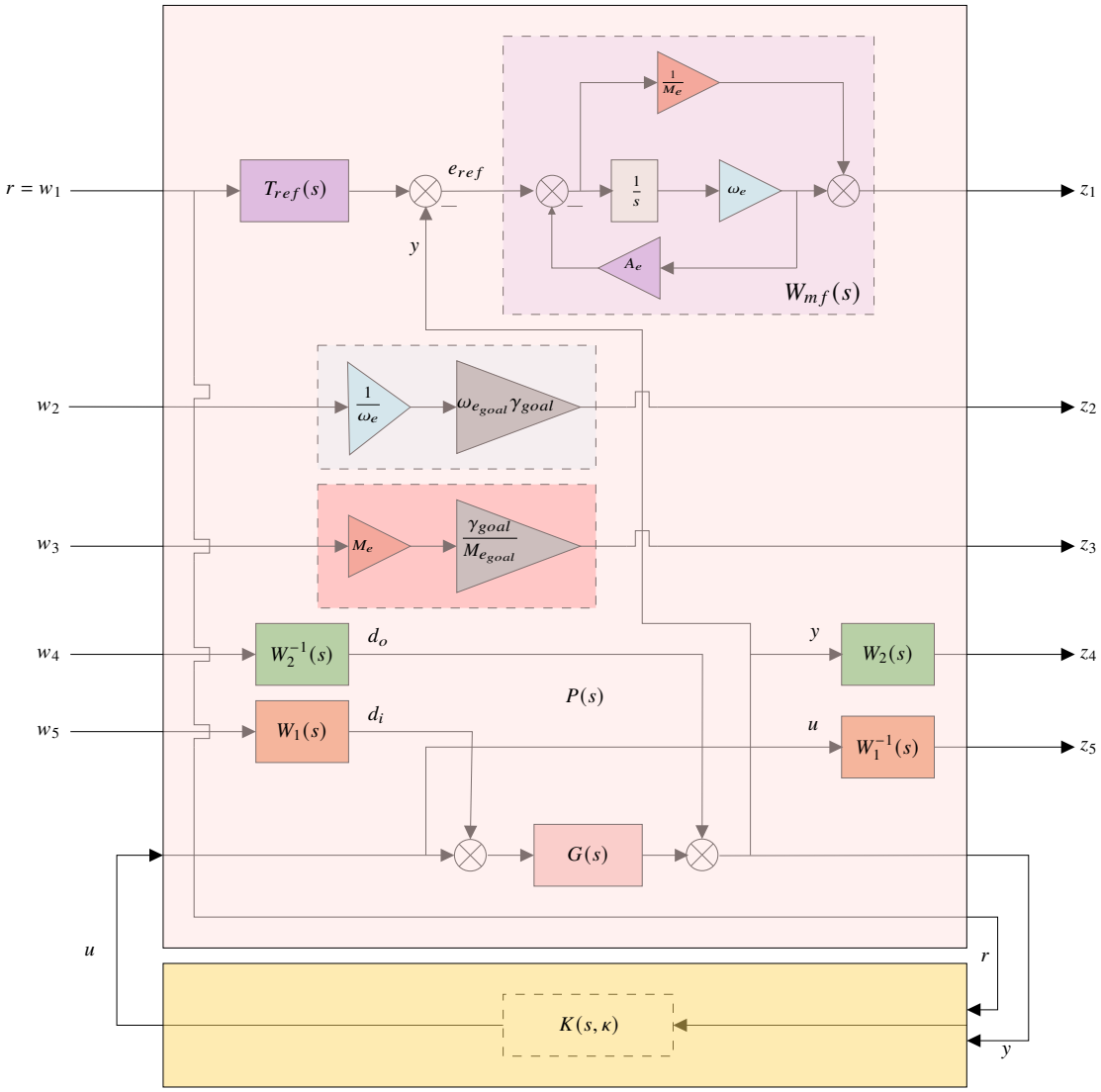

Fig. 11 General description of non-smooth non-convex $\mathcal{H}_\infty$-synthesis under controller structural constraints against multiple requirements using the $\mathcal{H}_\infty$ LSDP and a co-design procedure for model-following requirements.

Dynamic Inversion controllers [28]. The proposed framework offers a systematic and transparent methodology to design flight control laws with robustness guarantees while offering flexibility for the control structure to be chosen a priori.

C. Digital Design Extensions

Control laws are usually implemented in digital form. These digital, or discrete-time, controllers include discretization effects that should be accounted for in the continuous-time design [52]. The approach adopted in this study is referred to as modified continuous design and it takes into consideration the properties of the sampling process and also the computational delays by modifying the continuous-time controller to include continuous-time models which approximate these digital effects. This results in the discretized controller and the modified continuous controller yielding a more similar response [52].

There are multiple elements used to simulate the interaction between a continuous-time plant and a discrete-time controller, such as zero-order hold (ZOH), computational delays, and analogue-to-digital (A/D) converters [52]. In order to model these effects using continuous-time transfer functions, the following approximations are used to model the ZOH, computational delay and anti-aliasing filter, respectively:

$$G_{ZOH}(s) = \frac{1 - e^{-sT_s}}{sT_s},\ G_{del}(s) = e^{-s\Delta},\ G_{alias}(s) = \frac{a}{s+a} \tag{23}$$

However, the approximations of the ZOH and of the computational delay are not rational; thus, Padé approximants of $e^{-s\Delta}$ and e^{-sT} are used to approximate these effects via rational transfer functions [52]:

$$G_{ZOH}(s) = \frac{1 - e^{-sT_s}}{sT_s} \approx \frac{1}{1 + sT_s/2} \tag{24}$$

$$G_{del}(s) = e^{-s\Delta} \approx \frac{1}{1 + s\Delta} \tag{25}$$

In order to design a continuous controller which takes into consideration these multiple discretization and anti-aliasing effects, these are re-imagined as being part of the plant G to be controlled in Fig. 11. By doing so, the deterioration of the maximum attainable robustness margin due to these effects is directly reflected by computing $\epsilon_{\max} = \gamma_{\min}^{-1}$ (see Equation 12) for the shaped plant $G_s = W_2 G W_1$. The anti-aliasing filter is usually implemented using analogue circuitry, while $G_{del}(s)$ is not explicitly implemented since it is a model of the computation delay and $G_{ZOH}(s)$ is implemented by the ZOH and the sampler.

D. Summary: Framework for Tuning Incremental Dynamic Inversion Controllers Using the $\mathcal{H}_\infty$ LSDP

The current section summarizes the above sections into a framework to tune Incremental Dynamic Inversion Controllers for SISO systems using the $\mathcal{H}_\infty$ Loop-Shaping Design Procedure:

1) Translate the multiple design requirements into a reference model T_{ref} according to model-following requirements.
2) Follow the general guidelines of $\mathcal{H}_\infty$ LSDP to define the desired shaping G_s and compute W_1 and W_2 accordingly. Take into consideration the lower and upper bounds imposed by RHP poles and zeros, respectively, on the crossover frequency ω_{co}.*
3) Compute the theoretical $\gamma_{\min}$ associated with the shaped plant $G_s = W_2 G W_1$.† According to literature, an adequate value for $\gamma_{\min}$ lies between 1 and 4 [33]. Otherwise, the performance specified via the weighting filters W_1 and W_2 is not compatible with a robust design and the filters need to be redesigned.
4) Employ the 1 DoF procedure outlined in [47] (optimizing only for robust stability) to evaluate if Hypothesis 1 holds, by using an optimization solver capable of solving structured $\mathcal{H}_\infty$ problems, such as MATLAB® `systune`.
5) If the previous step is successful (obtained γ is close to $\gamma_{\min}$), move to a 2DoF setup where model-following performance is imposed via a model-following weighting filter on the tracking error signal.
6) **OPTIONAL:** Employ a co-design approach, where the model following weighting filter W_{mf} is optimized simultaneously with the IDI controller. This requires the designer to define a target bandwidth $\omega_{e_{goal}}$ and peak value $M_{e_{goal}}$ of W_{mf}, and target robustness level γ_{goal}. This is how the designer can trade-off performance and robustness.

IV. Design Case Study

In this section, the methodology outlined in the preceding sections is demonstrated in a design case study focused on a longitudinal flight control augmentation system, namely a digital pitch-rate controller, for a simulation model of the X-29 research aircraft. In a previous study with a 1DoF design, [47] shows that the hybrid IDI control structure is compatible with the $\mathcal{H}_\infty$ Loop-Shaping controller for this case-study. Therefore, having verified that Hypothesis 1 holds, this study will directly address the 2DoF digital case, where model-following performance requirements are introduced and the controller is implemented in digital form.

The X-29 was a forward-swept-wing former NASA research airplane, which was built to demonstrate aerodynamic performance improvements that might be gained from new composite materials. It constitutes a particularly interesting

*It is important to highlight that W_1 and W_2 will not incorporate the final controller, and so their complexity can be increased without increasing the complexity of the final controller, whose structure is fixed to one of the selected Incremental Dynamic Inversion architectures. On one hand, this allows to better shape of the open-loop plant, but on the other hand, it is important to keep in mind that the procedure builds on Hypothesis 1 that states that $K_{struct} \rightarrow K_s$, which means that unnecessary inflating the order of the weighting filters can lead to a design which is incompatible with the fixed tunable elements in the structured IDI controller.

†For digital control design, a modified continuous design can be adopted, where the different discretization effects are modeled as continuous-time models and are re-imagined as part of the open-loop plant G.

Table 1 Short-period model coefficients for the flight condition M = 0.9 and h = 8000ft.

Parameters	Z_α (s^{-1})	1+Z_q/V_o (-)	M_α (s^{-2})	M_q (s^{-1})	Z_δ (s^{-1})	M_δ (s^{-2})
Value	-2.241	0.9897	44.74	-0.9024	-0.2331	-45.93

case study due to its fundamental control limitations [53]. The Linear Time Invariant (LTI) short-period model used for the synthesis and analysis is described in Section IV.A. The flight control system is described IV.B and the derivation of the reference model based on handling qualities is explained in Section IV.C. The optimization setup, which includes designing the weighting filters and defining the co-design parameters, and the resulting synthesis results are given in Section IV.D. Lastly, simulation results of a digital implementation of the hybrid IDI controller are presented in Section IV.E.

A. X-29 Model

The flight condition (M = 0.9 and altitude = 8000 ft) chosen for the controller's design is challenging due to the plane's violent instability, which results in the longitudinal open-loop system having an unstable pole at p = 5.12 rad/s. The aircraft has three longitudinal inputs: a canard, a symmetric flap, and a strake flap. However, for simplicity, the short-period dynamics model used is retrieved from [54], where a linear combination of the three inputs is used to achieve a single virtual input δ_e, resulting in the following nominal system with values specified in Table 1:

$$\begin{bmatrix} \dot{\alpha} \\ \dot{q} \end{bmatrix} = \begin{bmatrix} Z_\alpha & 1 + Z_q/V_o \\ M_\alpha & M_q \end{bmatrix} \begin{bmatrix} \alpha \\ q \end{bmatrix} + \begin{bmatrix} Z_\delta \\ M_\delta \end{bmatrix} \delta_e \tag{26}$$

In order to model the actuator dynamics, a second-order transfer function is used, with ω_n = 70 rad/s and ξ = 0.7 [54].

$$G_{act}(s) = \frac{\delta_e(s)}{\delta_{e_{cmd}}(s)} = \frac{\omega_n^2}{s^2 + 2\xi\omega_n s + \omega_n^2} = \frac{70^2}{s^2 + (2)(0.7)(70)s + 70^2} \tag{27}$$

The unstable RHP pole of the short-period model imposes a lower bound on the allowed complementary sensitivity T bandwidth ω_{BT}, with an approximate bound of $\omega_{co} > 2p$ [40]. Therefore, the crossover frequency of the shaped plant G_s should be made to be at least $\omega_{co} > 2p$ = 10.24 rad/s.

B. Flight Control System

The X-29 is a prime example of how hardware limitations impose limits on what the control system can achieve, due to the limited available bandwidth. The flight control computer featured an 80 Hz sampling rate that was split in half for each control channel: longitudinal and lateral [55]. As a result, the longitudinal controller had a sampling frequency of 40 Hz, or, in other words, a sampling time T_s = 0.025s. Additionally, reports claim that the computational delay Δ was, on average, 10 ms [55]. Given that the sampling frequency for the longitudinal controller channel is 40 Hz, the Nyquist frequency is equal to 20 Hz. Thus, the anti-aliasing filter cutoff frequency was selected to be 19 Hz in this study, just below the Nyquist frequency. The computation delay and the ZOH plus sampler were modeled using first-order Padé approximations as described in Equations 24 and 25:

$$G_{ZOH}(s) = \frac{80}{s+80},\ G_{del}(s) = \frac{100}{(s+100)},\ G_{alias}(s) = \frac{119.38}{s+119.38} \tag{28}$$

1. Hybrid IDI Control Law Architecture

The general hybrid IDI control architecture is defined in Fig. 9. For this case study, the outer-loop controller $K_v(s)$ is defined as a PI controller in series with a first-order low-pass filter (LPF). In terms of the hybrid inversion elements, K_c is a scaling gain bounded between [0,1] and the compensation filter $H_c(s)$ is set as a first-order LPF to maintain a good degree of commonality with previous related studies [31, 47].

$$K_v(s) = \frac{K_p(s + K_i/K_p)}{s} \frac{\omega_{lp}}{s + \omega_{lp}} \tag{29}$$

$$H_c(s) = \frac{\omega_c}{s + \omega_c} \tag{30}$$

Moreover, given that model-based DI control requires full-state feedback for the inversion, a basic angle-of-attack estimator based on the short-period model information is introduced:

$$\hat{x}(s) = \left[\hat{\alpha}(s)\ q(s)\right]^T = F(s)\ q(s) = \left[\frac{1+Z_q/V_o}{s-Z_\alpha} \quad 1\right]^T q(s) \tag{31}$$

Given the challenges that arise due to the reduced sampling rate available to control a highly unstable aircraft, a second-order feedforward compensator is selected:

$$K_{ff}(s) = K\frac{(s+z_1)(s+z_2)}{s^2 + 2\xi\omega_n s + {w_n}^2} \tag{32}$$

Since the maximum frequency of the controller poles should be well beneath the Nyquist frequency, a maximum value of 12.5 Hz was chosen. Additionally, since the poles of the feedforward controller will directly appear as poles of the closed-loop system, a minimum damping of 0.707 was imposed to these poles.

C. Choice of Reference Model Based on Handling Qualities

The nature of the operational mission is directly linked to the formulation of the flight control law design goals. In this context, [49] specifies aircraft class designation (I-IV) and identifies different flight phases (A-C). Under this criteria, the X-29 aircraft falls within Class IV and the flight conditions used lie within Flight Phase Category A. The flying quality levels can be classified into three different levels (I-III), and it is desired to accomplish Level I satisfactory flying quality levels across the operational flight envelope.

Based on this, [49] describes desired modal response characteristics. The high-order pitch rate frequency response of a classical aircraft to an elevator input can be approximated by the following LOES:

$$\frac{q(s)}{\delta_e(s)} = \frac{K_q\left(s + \frac{1}{T_{\theta_2}}\right)e^{-\tau_e s}}{s^2 + 2\xi\omega_n s + \omega_n^2} \tag{33}$$

The Control Anticipation Parameter (CAP) and the Gibson's dropback criterion were used to define the multiple parameters that comprise $T_{ref}(s)$, similarly to what was done in [56].

The CAP serves as a physical measure of an aircraft's maneuverability. It reflects the relationship between the initial pitching acceleration and the steady-state normal g-force experienced after a step input to the controls. This criterion highlights how a pilot's ability to predict the aircraft's flight path response is directly tied to this ratio [57]. The CAP can be described in terms of the variables of the LOES as in Equation 34.

$$CAP = \frac{\dot{q}(0)}{n_z(\infty)} \approx \frac{g\omega_{sp}^2 T_{\theta_2}}{V_{TAS}} \tag{34}$$

The Gibson's dropback criterion is defined by limiting two key parameters: the pitch rate overshoot ratio $\frac{q_m}{q_s}$ and the ratio of attitude dropback (or overshoot, depending on the direction of the transition when the step input is removed) to the steady-state pitch rate [57]. It can be described in terms of the variables of the LOES as follows:

$$\mathrm{DB}/q_{ss} = T_{\theta_2} - \frac{2\xi}{\omega_n} \tag{35}$$

Thus, by choosing a point that adheres to Level I flying qualities in the CAP criteria and a point that lies within the frame of satisfactory flying qualities in Gibson's dropback criteria, the designer sets the desired CAP_{ref}, and $(DB/qss)_{ref}$. The desired damping of the response ξ_{ref} is also directly set by the designer. From this, it is possible to solve the system of equations in Equation 36 and compute ω_{ref} and $T_{\theta_{2_{ref}}}$, similarly to what was done in [56]. Regarding the remaining parameters, $K_{q_{ref}}$ is chosen such that T_{ref} has unitary static gain, and since the reference model is a pure second-order system, the equivalent time delay $\tau_{e_{ref}}$ is zero.

$$\begin{cases} \mathrm{CAP} = \dfrac{g\,\omega_n\,T_{\theta_2}}{V_{TAS}} \\ \mathrm{DB}/q_{ss} = T_{\theta_2} - \dfrac{2\xi}{\omega_n} \end{cases} \tag{36}$$

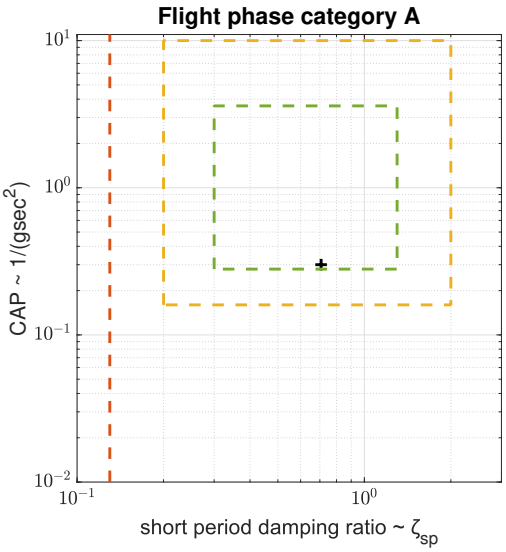

Fig. 12 Chosen point for the CAP criteria.

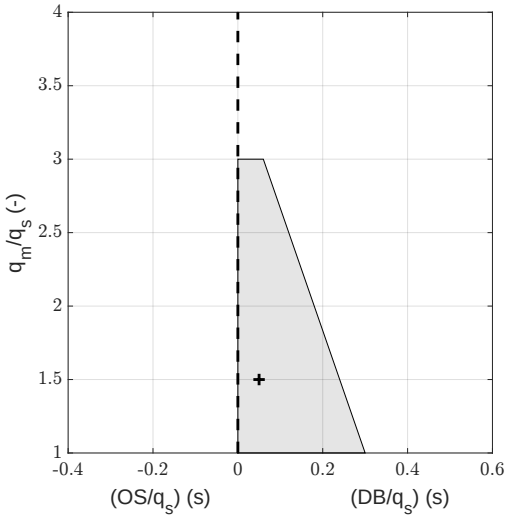

Fig. 13 Chosen point for the Gibson criteria.

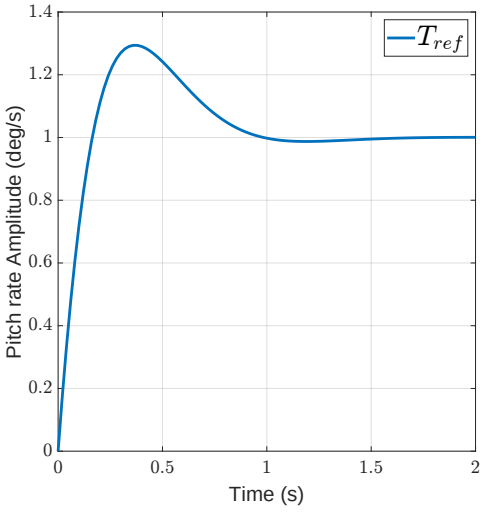

Fig. 14 Step response of T_{ref}.

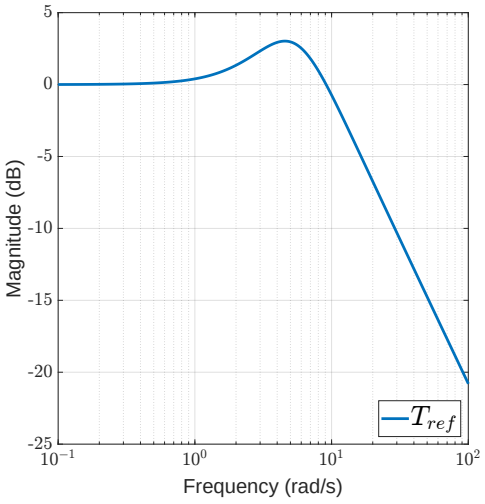

Fig. 15 Singular Values of $T_{ref}(s)$.

Consequently, T_{ref} is described as:

$$T_{ref}(s) = \frac{q(s)}{\delta_e(s)} = (\omega_n^2)(T_{\theta_2})\frac{s + \frac{1}{T_{\theta_2}}}{s^2 + 2\xi\omega_n s + \omega_n^2} \tag{37}$$

The desired short-period damping was directly set as $\xi = 0.707$, and points in the CAP and Gibson criteria were chosen as shown in Fig. 12 and Fig. 13. Solving the system of equations in Equation 36, resulted in the reference model T_{ref} in Equation 38 and Fig. 14-15.

$$T_{ref} = \frac{9.12(s + 3.21)}{s^2 + (2)(0.707)(5.41)s + (5.41)^2} \tag{38}$$

Table 2 Shaping filters and Co-Design setup.

	Shaping Filters		Co-Design setup			
Parameter	W_1	W_2	γ_{goal}	$\omega_{e_{goal}}$	$M_{e_{goal}}$	A_e(fixed)
Value	$\frac{0.3121(s+9)}{s}$	1	3.3	50	1	0.0032

Table 3 Optimized values for the multi-objective tuning goals, where the minimum attainable γ_{th} is included for comparison.

	NCF Robustification (Soft)		Co-Design (Soft)		Model-Following (Hard)
Tuning Goal	γ_{th}	γ	ω_e	M_e	W_{mf}
Value ($\mathcal{H}_\infty$-norm)	2.90	3.52	3.52	3.52	1.00

Table 4 Optimized gains of the digital hybrid IDI and of the Co-Design parameters of W_{mf}.

	Virtual Control			Inversion Loop		Feedforward	MF Filter W_{mf}		
Parameter	K_p	K_i	ω_{lp}	K_c	ω_c	K_{ff}	A_e	ω_e	M_e
Value	5.33	8.79	13.94	0.77	22.38	$\frac{28.94(s^2+16.96s+213.2)}{(s^2+110s+6166)}$	0.0032	46.92	1.07

D. Optimization Setup & Results

The total open-loop plant G_{ol} is given by a series interconnection of the computational delay model, the ZOH model, the actuator dynamics, the transfer-function from the virtual input to pitch-rate G_{sp} and the anti-aliasing filter:

$$G_{ol}(s) = G_{alias}(s)G_{sp}(s)G_{act}(s)G_{ZOH}(s)G_{del}(s) \tag{39}$$

Given the lower-bound imposed on the crossover frequency due to the RHP pole ($\omega_{co} > 10.24$ rad/s), it was set at around 13.5 rad/s. In order to boost the low-frequency gain of the open-loop plant G_{ol}, obtain a -20 dB slope around crossover, and attain the minimum desired crossover frequency, W_1 was set as a PI, while, for simplicity, W_2 was set to 1.

$$W_1 = K_p + \frac{K_i}{s} = \frac{0.3121(s+9)}{s} \tag{40}$$

The resulting shaped plant $G_s = W_2 G_{ol} W_1$ fulfills the desired shaping, as can be observed in Fig. 17. In order to assess whether the following shaping of the plant is compatible with a robust design, a suboptimal $\gamma_{th} > \gamma_{\min}$ is computed with the common default tolerance of 1e-3. The resulting $\gamma_{th} = 2.90$ adheres to the common guideline that sets an acceptable range for γ between 1 and 4 [58].

The following step is to define the model-following weighting filter. A co-design approach was used, as described in Section III.B.2, where the target bandwidth was set as $\omega_{e_{goal}} = 50$, the target peak value as $M_{e_{goal}} = 1$, and the target robustness level as $\gamma_{goal} = 3.3$.

An overview of the weighting filters and the co-design parameters are displayed in Table 2. The structured hybrid IDI controller is then optimized using the optimization setup described in Equation 22 in MATLAB® `systune`. The synthesis results in terms of the multi-objective tuning goals and the optimized controller gains are displayed in Tables 3 and 4 respectively. Model-following performance results are depicted in Fig. 16 and robustness analysis results are displayed in Section IV.D.1.

In terms of the model-following objectives, the co-design tuning goals have the same value as γ, which corroborates that these constraints were adequately scaled to be competitive with the NCF robustification one. For instance, making $\omega_{e_{goal}}$ larger would result in prioritizing more model-following performance, but it would come at the cost of a higher γ. Therefore, a compromise was made between robustness and performance.

One of main synthesis outcomes is that the optimization took advantage of the hybrid inversion architecture, which is reflected by the intermediate value of the scaling gain K_c. Moreover, from Fig. 16a, it is possible to attest to the

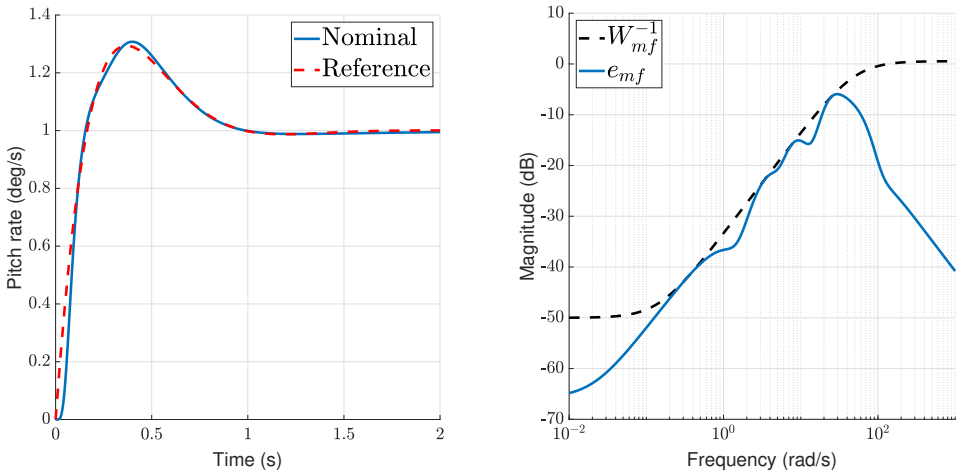

(a) Pitch rate step-tracking performance. **(b) Singular values of model-following error.**

Fig. 16 Model-following performance.

success of the feedforward element in achieving good model-following performance, given that the pitch rate response to a step input closely matches the reference model T_{ref} response. The model following error is tightly bound by W_{mf}^{-1}, as can be seen in Fig. 16b. This is expected, given the model-following hard constraint value of 1.00.

1. Robustness Analysis

From the input broken-loop response in Fig. 18, it can be observed that the singular values of the broken-loop response is very similar to the shaped plant G_s. This is a typical property of the $\mathcal{H}_\infty$ LSDP and hints at the success of the design procedure to tune a hybrid IDI using the $\mathcal{H}_\infty$ LSDP. Moreover, the broken-loop response is very much identical to the broken-loop response of the controlled system with the standard full-order $\mathcal{H}_\infty$ Loop-Shaping controller using the same weighting filters, which is another indicator of the success of the synthesis procedure. In terms of the 'gang-of-six' closed-loop transfer functions exhibited in Fig. 19a-19d, it can be seen that they exhibit the desired behavior, namely, low-gain at low-frequencies for the sensitivity function S_i and for SoG, low-gain at high-frequencies

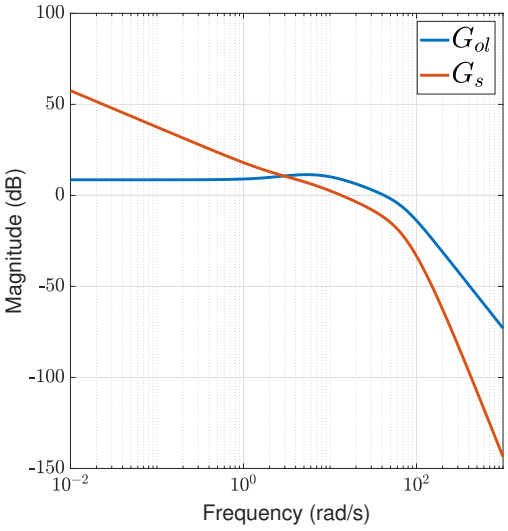

Fig. 17 Singular values of open-loop plant G_{ol} and shaped plant G_s.

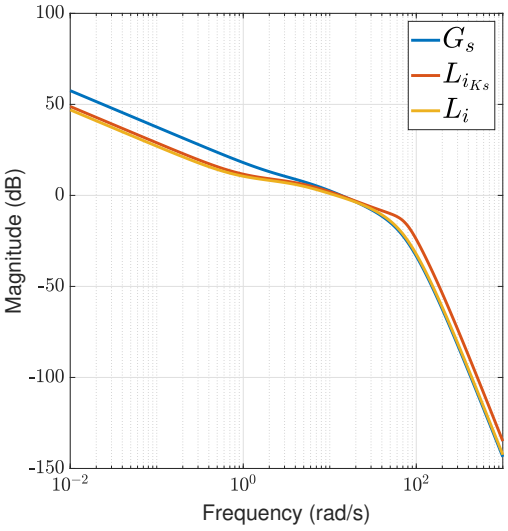

Fig. 18 Broken-loop response at plant input L_i of full-order $\mathcal{H}_\infty$ LS controller K_s and the tuned H-IDI controller.

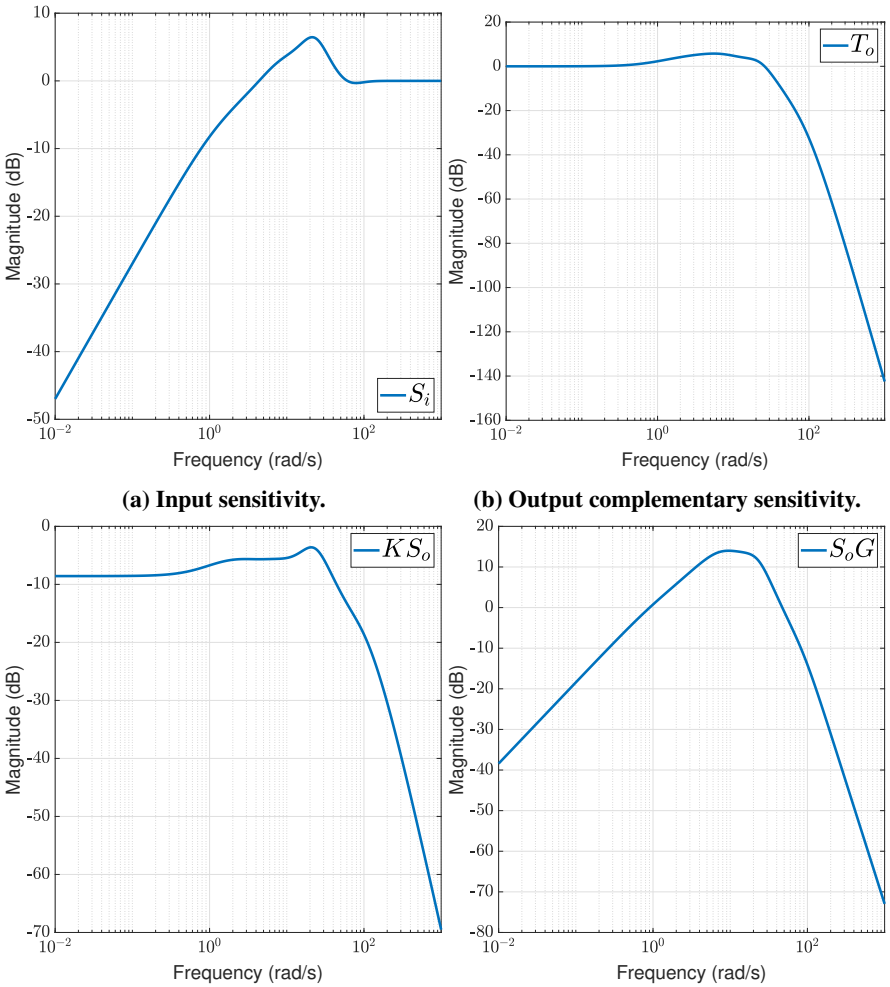

(a) Input sensitivity. **(b) Output complementary sensitivity.**

(c) Controller times the output sensitivity. **(d) Output sensitivity times the plant.**

Fig. 19 Singular values of the "gang-of-six" transfer functions.

for the complementary sensitivity function T_o and control signal attenuation at high frequencies (low-gain of KS_o at high-frequencies). Since it is a SISO system, S_o and T_i are not plotted because they are redundant.

Nevertheless, inspecting the classical gain and phase margins and the disk-margins (see Fig. 20) displayed in Table 5, it can be seen that they are below the standard requirement for certification of a minimum of 6 dB of gain margin and 45° of phase margin. However, as pointed out in [53], control systems have fundamental limitations according to the limitations of the hardware and the instability of the open-loop plant. The author demonstrates, using Bode integral relationships, that the X-29, at an even more unstable condition with a pole at 6 rad/s, has a maximum attainable phase margin of 35°. The flight condition considered in this study is similarly unstable. Thus, the obtained value for the PM of 35° is in accordance with the X-29's stability margins measured in flight [59].

Table 5 Classical and Disk-based margins for the digital hybrid IDI design.

	Classical	Disk-based		
		S-T ($\sigma = 0$)	S ($\sigma = 1$)	T ($\sigma = -1$)
GM (dB)	[-7.5, 7.1]	[-5.3, 5.3]	[-3.4, 5.6]	[-6.3, 3.6]
PM (°)	35.3	±32.9	±27.5	±29.9

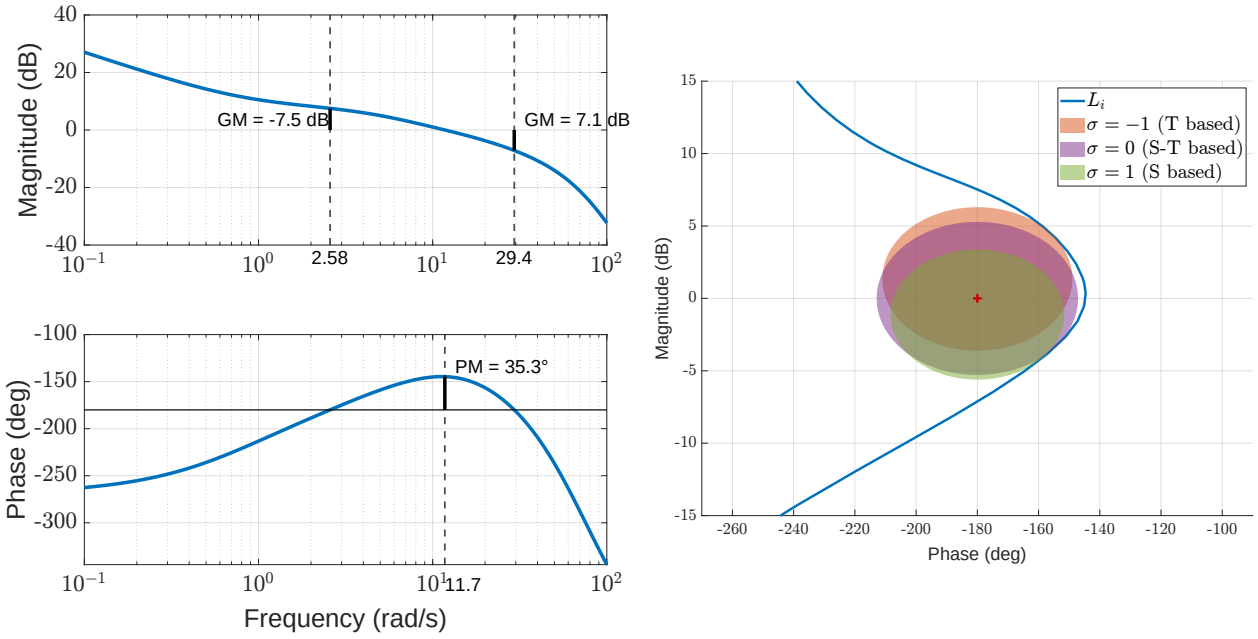

Fig. 20 Bode plot and Nichols plot of input broken-loop frequency response with disk-based exclusion regions.

E. Digital Implementation

The hybrid inversion schematic presented in Fig. 9 can be implemented as a scaling complementary filter as proposed in [31, 32] and depicted in Fig. 21. This implementation is advantageous since it does not require explicit signal differentiation of the output signal y. Using this architecture, the outer and inner loop controller can be implemented using only the gains K_p, K_i, ω_{lp}, K_c, ω_c and discrete integrators. The only elements that need to be discretized are the feedforward element and the integrators. In order to do so, the bilinear transform, also known as Tustin's method, was used using the sampling time of T_s = 25 ms based on the X-29 sampling rate, which resulted in the discrete-time controller shown in Equation 41 [52].

$$K_{ff}(z) = \frac{10.8 - 16.76z^{-1} + 7.12z^{-2}}{1 - 0.02186z^{-1} + 0.1765z^{-2}} \tag{41}$$

The controlled system response to pitch-rate command signals with the digital hybrid IDI controller (running at a sampling time of 25 ms) is compared with the the modified continuous-time hybrid IDI controller (which is simulated in

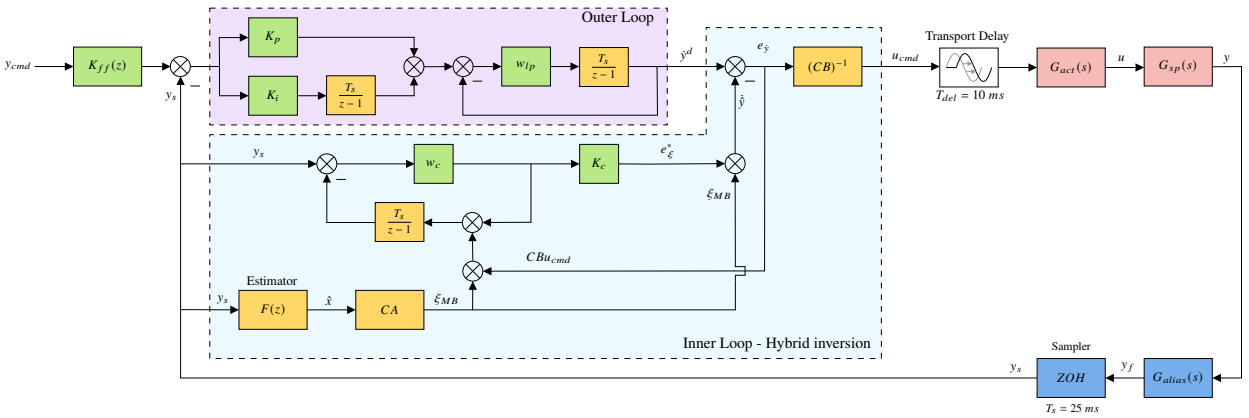

Fig. 21 Digital implementation of the hybrid IDI controller; the green blocks correspond to the tunable elements of the controller.

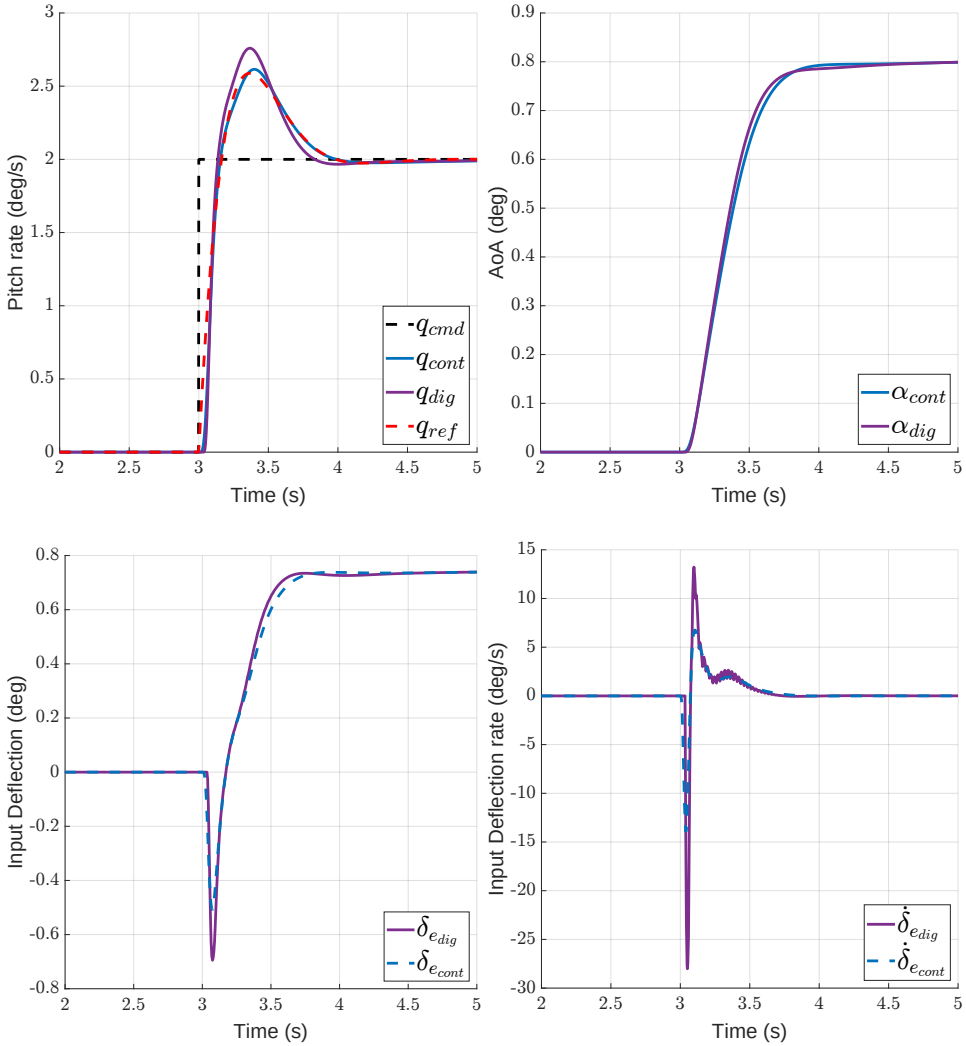

Fig. 22 Comparison of pitch-rate, AoA, input deflection and deflection-rate response between continuous and digital control simulation for pitch-rate step command at t = 3s.

continuous-time). In order to simulate the computational delay, a transport delay was implemented with delay equal to 10 ms. Simulation results of a comparison between the digital control simulation and the modified continuous controller used for the synthesis are displayed in Fig. 22.

The pitch-rate response with the digital controller overshoots slightly compared with the pitch-rate response of the continuous controller and of the reference model. This behavior arises primarily because the discrete-time feedforward controller does not fully reproduce the dynamics of its continuous-time counterpart at the chosen sampling rate. For instance, if a 10 ms sampling time (100 Hz sampling frequency) was used, then the response of the pitch rate with the digital controller would be identical to the continuous controller, as shown in Fig. 23.

The limitations imposed by low-sampling times are much less of an issue on modern flight control applications, given the higher sampling rates of flight control computers [60]. Nevertheless, the X-29 provides an insightful case study, given that its high instability and limited available bandwidth demand careful consideration of robustness and performance trade-offs. The proposed methodology manages these trade-offs by employing a co-design approach which allows to directly weight robust stability against model-following performance.

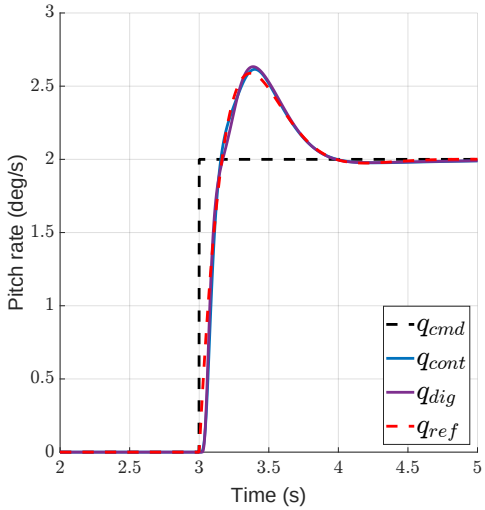

Fig. 23 Comparison of pitch-rate response between continuous and digital control simulation for pitch-rate step command at t = 3s with T_s=10ms.

V. Conclusion

This study presented a design framework to tune hybrid Incremental Dynamic Inversion (IDI) controllers using the $\mathcal{H}_\infty$ Loop-Shaping Design Procedure. It leverages non-smooth non-convex $\mathcal{H}_\infty$ optimization to tune the structured controller with the robustness guarantees associated with the $\mathcal{H}_\infty$ Loop-Shaping technique. The procedure can be used for other structured controller architectures under the Hypothesis that it has a compatible structure to that of full-order controller $K_s = W_1 K_\infty W_2$ associated with the $\mathcal{H}_\infty$ Loop-Shaping solution. The framework is evaluated in a design case study focused on a digital pitch-rate controller for a simulation model of NASA's X-29 experimental aircraft.

The synthesis procedure uses a two-degree-of-freedom control setup where model-following specifications are included and a feedforward is added to the hybrid IDI controller. Nominal performance is specified via minimization of a weighted $\mathcal{H}_\infty$ norm of the error signal between the output and the reference model signal. Flying qualities and handling qualities specifications are implemented in terms of the modal parameters of Low-Order Equivalent System (LOES) models via reference models T_{ref}. Multi-objective $\mathcal{H}_\infty$-synthesis in MATLAB® `systune` was used to employ a co-design approach in which the controller and the model-following filter parameters are optimized simultaneously, making the overall procedure more streamlined.

The design of a digital pitch-rate controller for the X-29 aircraft constitutes a relevant case study, given the highly unstable nature of the plane and the hardware limitations which compromise the attainable robustness margins. The proposed synthesis procedure offers a systematic and transparent way to trade-off robustness and performance by allowing the designer to directly weigh robustness against performance via the co-design approach described.

While the framework proposed in this work explicitly addresses nominal performance requirements, further research is required to extend it to include robust performance requirements. Furthermore, the synthesis framework was limited to an LTI context. Since (I)NDI control is intrinsically a nonlinear controller, the nonlinear nature of the plant is not reflected in the tuning process. How to achieve consistent robustness properties, often based on local robustness tests, across a wide flight envelope is still an undergoing research direction. Further investigation to structured Linear Parameter-Varying (LPV) synthesis is therefore recommended to address this challenge.

References

[1] Harris, J., "F-35 Flight Control Law Design, Development and Verification," *2018 Aviation Technology, Integration, and Operations Conference, Atlanta, Georgia, USA*, 2018, p. 3516. https://doi.org/10.2514/6.2018-3516.

[2] Hyde, R., *H_∞ Aerospace Control Design: A VSTOL Flight Application*, Advances in Industrial Control (AIC), Springer London, 1995. https://doi.org/10.1007/978-1-4471-3049-9.

[3] Miller, C., "Nonlinear Dynamic Inversion Baseline Control Law: Architecture and Performance Predictions," *AIAA Guidance, Navigation and Control Conference, Portland, Oregon, USA*, 2011, p. 6467. https://doi.org/10.2514/6.2011-6467.

[4] Miller, C., "Nonlinear Dynamic Inversion Baseline Control Law: Flight-Test Results for the Full-scale Advanced Systems Testbed F/A-18 Airplane," *AIAA Guidance, Navigation and Control Conference, Portland, Oregon, USA*, 2011, p. 6468. https://doi.org/10.2514/6.2011-6468.

[5] Canin, D., "F-35 High Angle of Attack Flight Control Development and Flight Test Results," *AIAA aviation 2019 forum, Dallas, Texas, USA*, 2019, p. 3227. https://doi.org/10.2514/6.2019-3227.

[6] Hyde, R., and Papageorgiou, G., "Analysing the stability of NDI-based flight controllers with LPV methods," *Proceedings of the AIAA Guidance, Navigation and Control Conference, Montreal, Canada*, 2001. https://doi.org/10.2514/6.2001-4039.

[7] Pollack, T., and van Kampen, E., "Robust Stability and Performance Analysis of Incremental Dynamic-Inversion-Based Flight Control Laws," *Journal of Guidance, Control, and Dynamics*, Vol. 46, No. 9, 2023, pp. 1785–1798. https://doi.org/10.2514/1.G006576.

[8] Smith, P., "A Simplified Approach to Nonlinear Dynamic Inversion Based Flight Control," *23rd Atmospheric Flight Mechanics Conference, Boston, Massachusetts, USA*, 1998, p. 4461. https://doi.org/10.2514/6.1998-4461.

[9] Smith, P., and Berry, A., "Flight test Experience of a Non-linear Dynamic Inversion Control Law on the VAAC Harrier," *Atmospheric Flight Mechanics Conference, Denver, Colorado, USA*, 2000. https://doi.org/10.2514/6.2000-3914.

[10] Bacon, B., and Ostroff, A., "Reconfigurable Flight Control Using Nonlinear Dynamic Inversion with a Special Accelerometer Implementation," *AIAA Guidance, Navigation, and Control Conference and Exhibit, Denver, Colorado, USA*, 2000, p. 4565. https://doi.org/10.2514/6.2000-4565.

[11] Bacon, B., Ostroff, A., and Joshi, S., "Nonlinear Dynamic Inversion Reconfigurable Controller Utilizing a Fault Tolerant Accelerometer," *19th DASC. 19th Digital Avionics Systems Conference. Proceedings (Cat. No. 00CH37126), Philadelphia, Pennsylvania, USA*, Vol. 2, IEEE, 2000, pp. 6F5/1–6F5/8 vol.2. https://doi.org/10.1109/dasc.2000.884920.

[12] Bacon, B., Ostroff, A., and Joshi, S., "Reconfigurable NDI Controller Using Inertial Sensor Failure Detection & Isolation," *IEEE Transactions on Aerospace and Electronic Systems*, Vol. 37, No. 4, 2001, pp. 1373–1383. https://doi.org/10.1109/7.976972.

[13] Ostroff, A., and Bacon, B., "Enhanced NDI Strategies for Reconfigurable Flight Control," *Proceedings of the 2002 American Control Conference (IEEE Cat. No. CH37301), Anchorage, Alaska, USA*, Vol. 5, IEEE, 2002, pp. 3631–3636. https://doi.org/10.1109/acc.2002.1024492.

[14] Sieberling, S., Chu, Q., and Mulder, J., "Robust Flight Control Using Incremental Nonlinear Dynamic Inversion and Angular Acceleration Prediction," *Journal of Guidance, Control, and Dynamics*, Vol. 33, No. 6, 2010, pp. 1732–1742. https://doi.org/10.2514/1.49978.

[15] Simplício, P., Pavel, M., van Kampen, E., and Chu, Q., "An acceleration measurements-based approach for helicopter nonlinear flight control using Incremental Nonlinear Dynamic Inversion," *Control Engineering Practice*, Vol. 21, No. 8, 2013, pp. 1065–1077. https://doi.org/10.1016/j.conengprac.2013.03.009.

[16] Yang, Y., Wang, X., Zhu, J., Yuan, X., and Zhang, X., "Robust proportional incremental nonlinear dynamic inversion control of a flying-wing tailsitter," *Proceedings of the Institution of Mechanical Engineers, Part G: Journal of Aerospace Engineering*, Vol. 234, No. 16, 2020, pp. 2274–2295. https://doi.org/10.1177/0954410020926657.

[17] Lombaerts, T., Kaneshige, J., Schuet, S., Aponso, B. L., Shish, K. H., and Hardy, G., "Dynamic Inversion based Full Envelope Flight Control for an eVTOL vehicle using a Unified Framework," *AIAA Scitech 2020 Forum, Orlando, Florida, USA*, 2020, p. 1619. https://doi.org/10.2514/6.2020-1619.

[18] Smeur, E., Chu, Q., and De Croon, G., "Adaptive Incremental Nonlinear Dynamic Inversion for Attitude Control of Micro Air Vehicles," *Journal of Guidance, Control, and Dynamics*, Vol. 39, No. 3, 2016, pp. 450–461. https://doi.org/10.2514/1.g001490.

[19] Grondman, F., Looye, G., Kuchar, R. O., Chu, Q. P., and van Kampen, E., "Design and Flight Testing of Incremental Nonlinear Dynamic Inversion based Control Laws for a Passenger Aircraft," *2018 AIAA Guidance, Navigation, and Control Conference, Kissimmee, Florida, USA.*, 2018, p. 0385. https://doi.org/10.2514/6.2018-0385.

[20] Pollack, T., Looye, G., and Van der Linden, F., "Design and flight testing of flight control laws integrating incremental nonlinear dynamic inversion and servo current control," *AIAA Scitech 2019 Forum, San Diego, California, USA*, 2019, p. 0130. https://doi.org/10.2514/6.2019-0130.

[21] Smeur, E. J., Bronz, M., and De Croon, G. C., "Incremental Control and Guidance of Hybrid Aircraft Applied to a Tailsitter Unmanned Air Vehicle," *Journal of Guidance, Control, and Dynamics*, Vol. 43, No. 2, 2020, pp. 274–287. https://doi.org/10.2514/1.G004520.

[22] Wang, X., van Kampen, E., Chu, Q., and Lu, P., "Stability Analysis for Incremental Nonlinear Dynamic Inversion Control," *Journal of Guidance, Control, and Dynamics*, Vol. 42, No. 5, 2019, pp. 1116–1129. https://doi.org/10.2514/1.G003791.

[23] van't Veld, R., van Kampen, E., and Chu, Q. P., "Stability and Robustness Analysis and Improvements for Incremental Nonlinear Dynamic Inversion Control," *2018 AIAA Guidance, Navigation, and Control Conference, Kissimmee, Florida, USA*, 2018, p. 1127. https://doi.org/https://doi.org/10.2514/6.2018-1127.

[24] Cordeiro, R. A., Marton, A. S., Azinheira, J. R., Carvalho, J. R. H., and Moutinho, A., "Increased Robustness to Delay in Incremental Controllers Using Input Scaling Gain," *IEEE Transactions on Aerospace and Electronic Systems*, Vol. 58, No. 2, 2022, pp. 1199–1210. https://doi.org/10.1109/TAES.2021.3123215.

[25] Huang, Y., Zhang, Y., Pool, D. M., Stroosma, O., and Chu, Q., "Time-Delay Margin and Robustness of Incremental Nonlinear Dynamic Inversion Control," *Journal of Guidance, Control, and Dynamics*, Vol. 45, No. 2, 2022, pp. 394–404. https://doi.org/10.2514/1.G006024.

[26] Jiali, Y., and Jihong, Z., "An angular acceleration estimation method based on the complementary filter theory," *2016 IEEE International Instrumentation and Measurement Technology Conference Proceedings, Taipei, Taiwan*, IEEE, 2016, pp. 1–6. https://doi.org/10.1109/I2MTC.2016.7520548.

[27] Kim, C.-S., Ji, C.-H., Koh, G.-O., and Kim, B. S., "Stability Margin and Structural Coupling Analysis of a Hybrid INDI Control for the Fighter Aircraft," *International Journal of Aeronautical and Space Sciences*, Vol. 22, No. 5, 2021, pp. 1154–1169. https://doi.org/10.1007/s42405-021-00394-8.

[28] Kumtepe, Y., Pollack, T., and van Kampen, E., "Flight Control Law Design using Hybrid Incremental Nonlinear Dynamic Inversion," *AIAA SciTech 2022 Forum, San Diego, California, USA & Virtual*, 2022, p. 1597. https://doi.org/10.2514/6.2022-1597.

[29] Milz, D., May, M., and Looye, G., "Flight Testing Air Data Sensor Failure Handling with Hybrid Nonlinear Dynamic Inversion," *Proceedings of the 2024 CEAS EuroGNC conference, Bristol, UK*, 2024. https://doi.org/10.82124/CEAS-GNC-2024-082.

[30] Milz, D., May, M. S., Dias Martins, J. P., Kuchar, R., and Looye, G., "Failure Handling on a Split-Flap Ultralight General Aviation Aircraft with Hybrid Nonlinear Dynamic Inversion," *34th Congress of the International Council of the Aeronautical Sciences, ICAS 2024, Florence, Italy*, 2024. URL https://elib.dlr.de/206422/.

[31] Pollack, T., Theodoulis, S., and van Kampen, E., "Commonalities between robust hybrid incremental nonlinear dynamic inversion and proportional-integral-derivative flight control law design," *Aerospace Science and Technology*, Vol. 152, 2024. https://doi.org/10.1016/j.ast.2024.109377.

[32] Pollack, T., "Advances in Dynamic Inversion-based Flight Control Law Design: Multivariable Analysis and Synthesis of Robust and Multi-Objective Design Solutions," Ph.D. thesis, Delft University of Technology, 2024. https://doi.org/10.4233/uuid:28617ba0-461d-48ef-8437-de2aa41034ea.

[33] McFarlane, D., and Glover, K., "A Loop Shaping Design Procedure using H_∞ Synthesis," *IEEE Transactions on Automatic Control*, Vol. 37, No. 6, 1992, pp. 759–769. https://doi.org/https://doi.org/10.1109/9.256330.

[34] Prempain, E., and Postlethwaite, I., "Static H_∞ loop shaping control of a fly-by-wire helicopter," *Automatica*, Vol. 41, No. 9, 2005, pp. 1517–1528. https://doi.org/10.1016/j.automatica.2005.04.001.

[35] Papageorgiou, G., and Glover, K., "Design of a Robust Gain Scheduled Controller for the High Incidence Research Model," *Guidance, Navigation, and Control Conference and Exhibit, Portland, Oregon, USA*, 1999, p. 4276. https://doi.org/10.2514/6.1999-4276.

[36] Papageorgiou, G., Glover, K., D'Mello, G., and Patel, Y., "Taking robust LPV control into flight on the VAAC Harrier," *Proceedings of the 39th IEEE conference on decision and control (Cat. No. 00CH37187), Sydney, Australia*, Vol. 5, IEEE, 2000, pp. 4558–4564. https://doi.org/10.1109/CDC.2001.914633.

[37] Apkarian, P., and Noll, D., "Nonsmooth H_∞ Synthesis," *IEEE Transactions on Automatic Control*, Vol. 51, No. 1, 2006, pp. 71–86. https://doi.org/10.1109/TAC.2005.860290.

[38] Apkarian, P., and Noll, D., "The H_∞ Control Problem is Solved," *Aerospace Lab*, , No. 13, 2017, pp. pages 1–11. https://doi.org/10.12762/2017.al13-01.

[39] Khalil, H., *Nonlinear Systems*, Pearson Education, Prentice Hall, Upper Saddle River, NJ, 2002.

[40] Skogestad, S., and Postlethwaite, I., *Multivariable Feedback Control: Analysis and Design*, John Wiley & Sons, 2005.

[41] Glover, K., and McFarlane, D., "Robust stabilization of normalized coprime factors: An explicit H_∞ solution," *1988 American Control Conference*, IEEE, 1988, pp. 842–847. https://doi.org/10.23919/ACC.1988.4789839.

[42] Zhou, K., and Doyle, J. C., *Essentials of Robust Control*, Prentice hall Upper Saddle River, NJ, 1998.

[43] "Application of Multivariable Control Theory to Aircraft Control Laws, Final Report: Multivariable Control Design Guidelines," Tech. Rep. WL-TR-96-3099, Honeywell Technology Center and Lockheed Martin Skunk Works and Lockheed Martin Tactical Aircraft Systems, 1996.

[44] Enns, D., Bugajski, D., Hendrick, R., and Stein, G., "Dynamic inversion: an evolving methodology for flight control design," *International Journal of control*, Vol. 59, No. 1, 1994, pp. 71–91. https://doi.org/10.1080/00207179408923070.

[45] Papageorgiou, C., and Glover, K., "Robustness Analysis of Nonlinear Flight Controllers," *Journal of Guidance, Control, And Dynamics*, Vol. 28, 2005. https://doi.org/10.2514/1.9389.

[46] Hirwa, S., Feyel, P., Duc, G., and Sandou, G., "On Practical Fixed Order H_∞ Loop-Shaping," *2013 European Control Conference (ECC), Zurich, Switzerland*, IEEE, 2013, pp. 2837–2842. https://doi.org/10.23919/ECC.2013.6669324.

[47] Encarnação, L., Pollack, T., and Theodoulis, S., "Tuning Hybrid Incremental Dynamic Inversion Control Laws using $\mathcal{H}_\infty$ Loop-Shaping," *IFAC-PapersOnLine*, Vol. 59, No. 16, 2025, pp. 325–330. https://doi.org/10.1016/j.ifacol.2025.10.124.

[48] Pollack, T., Theodoulis, S., and Wang, X., "Quasi-LPV Transformations for Robust Gain Scheduling of Incremental Nonlinear Dynamic Inversion-based Controllers," *IFAC-PapersOnLine*, Vol. 59, No. 15, 2025, pp. 97–102. https://doi.org/10.1016/j.ifacol.2025.10.064.

[49] Anonymous, "Flying Qualities of Piloted Aircraft. MIL-STD-1797A," Tech. rep., US Department of Defense (DoD), 1990.

[50] Limebeer, D., Kasenally, E., and Perkins, J., "On the Design of Robust Two Degree of Freedom Controllers," *Automatica*, Vol. 29, No. 1, 1993, pp. 157–168. https://doi.org/10.1016/0005-1098(93)90179-w.

[51] Pérez, C. A., Theodoulis, S., Sève, F., and Goerig, L., "Automatic weighting filter tuning for robust flight control law design," *IFAC-PapersOnLine*, Vol. 55, No. 16, 2022, pp. 400–405. https://doi.org/10.1016/j.ifacol.2022.09.057.

[52] Stevens, B., Lewis, F., and Johnson, E., *Aircraft Control and Simulation: Dynamics, Controls Design, and Autonomous Systems*, John Wiley & Sons, 2015. https://doi.org/10.1002/9781119174882.

[53] Stein, G., "Respect the Unstable," *IEEE Control systems magazine*, Vol. 23, No. 4, 2003, pp. 12–25. https://doi.org/10.1109/MCS.2003.1213600.

[54] Lavretsky, E., and Wise, K. A., *Robust and Adaptive Control With Aerospace Applications*, Springer, 2024.

[55] Bosworth, J., *Linearized Aerodynamic and Control Law Models of the X-29A Airplane and Comparison With Flight Data*, National Aeronautics and Space Administration, Office of Management, Scientific and Technical Information Program, 1992. URL https://ntrs.nasa.gov/citations/19920009932.

[56] Baptista Marques, J. A., Stroosma, O., and Theodoulis, S., "Design and Simulator Evaluation of a Structured 2DoF H_∞ Loop-Shaping Control Law for a Business Jet," *AIAA SCITECH 2025 Forum, Orlando, Florida, USA*, 2025, p. 2242. https://doi.org/10.2514/6.2025-2242.

[57] Gibson, J., "Development of a design methodology for handling qualities excellence in fly by wire aircraft," Thesis, Delft University of Technology, The Netherlands, 1999. URL https://repository.tudelft.nl/record/uuid:6b564b35-cb74-436c-8c47-845bfbbb8b4d.

[58] Hyde, R., and Glover, K., "The Application of Scheduled H_∞ Controllers to a VSTOL Aircraft," *IEEE Transactions on Automatic Control*, Vol. 38, No. 7, 1993, pp. 1021–1039. https://doi.org/10.1109/9.231458.

[59] Gera, J., and Bosworth, J., "Dynamic Stability and Handling Qualities Tests on a Highly Augmented, Statically Unstable Airplane," *AIAA Guidance, Navigation and Control Conference, Monterey, California, USA*, 1987, p. 2258. https://doi.org/10.2514/6.1987-2258.

[60] Kim, C., Ji, C., Bang, J., Koh, G., and Choi, N., "A Survey on Structural Coupling Design and Testing of the Flexible Military Aircraft," *International Journal of Aeronautical and Space Sciences*, Vol. 25, No. 1, 2024, pp. 122–145. https://doi.org/10.1007/s42405-023-00643-y.